



**HAL**  
open science

# Recycled oceanic crust and marine sediment in the source of alkali basalts in Shandong, eastern China: Evidence from magma water content and oxygen isotopes

Jia Liu, Qun-Ke Xia, Etienne Deloule, Huan Chen, Min Feng

► **To cite this version:**

Jia Liu, Qun-Ke Xia, Etienne Deloule, Huan Chen, Min Feng. Recycled oceanic crust and marine sediment in the source of alkali basalts in Shandong, eastern China: Evidence from magma water content and oxygen isotopes. *Journal of Geophysical Research: Solid Earth*, 2015, 120, pp.8281-8303. 10.1002/2015JB012476 . insu-03619372

**HAL Id: insu-03619372**

**<https://insu.hal.science/insu-03619372>**

Submitted on 25 Mar 2022

**HAL** is a multi-disciplinary open access archive for the deposit and dissemination of scientific research documents, whether they are published or not. The documents may come from teaching and research institutions in France or abroad, or from public or private research centers.

L'archive ouverte pluridisciplinaire **HAL**, est destinée au dépôt et à la diffusion de documents scientifiques de niveau recherche, publiés ou non, émanant des établissements d'enseignement et de recherche français ou étrangers, des laboratoires publics ou privés.

Copyright

## RESEARCH ARTICLE

10.1002/2015JB012476

## Key Points:

- The magma water contents are high, and  $\delta^{18}\text{O}$  are mostly  $<5.7\text{‰}$
- The decoupling of  $\epsilon\text{Hf}$  and  $\epsilon\text{Nd}$  could be caused by marine sediments
- The subducted oceanic slab plays considerable role for Shandong basalts

## Supporting Information:

- Data Set S1
- Data Set S2
- Data Set S3
- Data Set S4
- Text S1 and S2, Figures S1 and S2, and Tables S1 and S2

## Correspondence to:

J. Liu and Q.-K. Xia,  
liujia08@ustc.edu.cn;  
qkxia@ustc.edu.cn

## Citation:

Liu, J., Q.-K. Xia, E. Deloule, H. Chen, and M. Feng (2015), Recycled oceanic crust and marine sediment in the source of alkali basalts in Shandong, eastern China: Evidence from magma water content and oxygen isotopes, *J. Geophys. Res. Solid Earth*, 120, 8281–8303, doi:10.1002/2015JB012476.

Received 26 AUG 2015

Accepted 22 NOV 2015

Accepted article online 27 NOV 2015

Published online 28 DEC 2015

## Recycled oceanic crust and marine sediment in the source of alkali basalts in Shandong, eastern China: Evidence from magma water content and oxygen isotopes

Jia Liu<sup>1</sup>, Qun-Ke Xia<sup>2</sup>, Etienne Deloule<sup>3</sup>, Huan Chen<sup>1,4</sup>, and Min Feng<sup>1</sup>

<sup>1</sup>CAS Key Laboratory of Crust-Mantle Materials and Environments, School of Earth and Space Science, University of Science and Technology of China, Hefei, China, <sup>2</sup>School of Earth Sciences, Zhejiang University, Hangzhou, China, <sup>3</sup>CRPG, UMR 7358, CNRS, Université de Lorraine, Vandoeuvre-les-Nancy, France, <sup>4</sup>UMET, UMR CNRS 8207, Université de Lille1, Villeneuve d'Ascq, France

**Abstract** The magma water contents and cpx  $\delta^{18}\text{O}$  values in alkali basalts from the Fuyanyshan (FYS) volcano in Shandong, eastern China, were investigated by an inverse calculation based on the water content of clinopyroxene (cpx) phenocrysts, the  $^{iv}\text{Al}_{\text{cpx}}$ -dependent water partitioning coefficient  $D_{\text{water}}^{\text{cpx/melt}}$ , and secondary ion mass spectrometer, respectively. The calculated water content ( $\text{H}_2\text{O}$  wt.) of magma ranges from 0.58% to 3.89%. It positively correlates with heavy rare earth element concentrations and bulk rock  $^{87}\text{Sr}/^{86}\text{Sr}$  ratios, and it negatively correlates with Nb/U ratios. However, it is not correlated with bulk Mg ( $\text{Mg\#} = 100 \times \text{Mg} / (\text{Mg} + \text{Fe})$ ) and  $(\text{La}/\text{Yb})_n$  ( $n$  represents primitive mantle normalization). Combined with the rather homogenous distribution of water content within cpx grains, these correlations indicate that the water variations among different samples represent the original magma signature, rather than results of a shallow process, such as degassing and diffusion. The  $\delta^{18}\text{O}$  of cpx phenocrysts varies from 3.6‰ to 6.3‰ ( $\pm 0.5\text{‰}$ , 2SD), which may be best explained by the involvement of components from the lower and upper oceanic crust with marine sediments within the mantle source. The  $\text{H}_2\text{O}/\text{Ce}$  ratios of the calculated melts range from 113 to 696 and form a positive trend with bulk rock  $^{87}\text{Sr}/^{86}\text{Sr}$ , which cannot be explained by the recycled Sulu eclogite or by the metasomatized lithospheric mantle. Our modeling calculation shows that the decoupling of  $\epsilon\text{Hf}$  and  $\epsilon\text{Nd}$  could be caused by the involvement of marine sediments. Combining the high Ba/Th ratios, positive Sr spikes, and low Ce/Pb ratios for the Fuyanshan basalts, we suggest that the hydrous nature of the FYS basalts was derived from the hydrous mantle transition zone with ancient sediments.

### 1. Introduction

Cenozoic basalts are widely distributed along the coastal provinces and adjacent offshore shelf of eastern China (Figure 1). They typically exhibit enriched concentrations of large ion lithophile elements, light rare earth elements (LREEs), Nb, and Ta. Their radiogenic Sr-Nd isotopes vary from 0.7025 to 0.7055 and 0.5123 to 0.5130, respectively [Zou *et al.*, 2000; Choi *et al.*, 2005; Y. G. Xu *et al.*, 2012], which are similar to the characteristics of typical oceanic island basalts (OIB). These radiogenic isotopic affinities vary regionally (Figure 1). During the past 30 years, a large amount of geochemical data, including major and trace element concentrations and Sr-Nd-Pb-Hf-O isotopic systems, has been collected from various volcanic rocks in East China to clarify the origins of these OIB-like signatures and infer geodynamical implications [Zhou and Armstrong, 1982; Peng *et al.*, 1986; Zhi *et al.*, 1990; Fan and Hooper, 1991; Liu *et al.*, 1994; Zou *et al.*, 2000, 2014; Niu, 2005; Tang *et al.*, 2006; Y. G. Xu *et al.*, 2005, 2012; Z. Xu *et al.*, 2014; Chen *et al.*, 2009; Zeng *et al.*, 2010, 2011; J. J. Zhang *et al.*, 2009; Z. M. Zhang *et al.*, 2009; Wang *et al.*, 2011; Z. Xu *et al.*, 2012; Zhang *et al.*, 2012; Hong *et al.*, 2013; Huang *et al.*, 2013; Sakuyama *et al.*, 2013; Chen *et al.*, 2015; Guo *et al.*, 2014; Li *et al.*, 2014; Zhao *et al.*, 2014; Wu *et al.*, 2014; Wang *et al.*, 2015].

However, until now, there has been no consensus. Various models have been suggested to explain the production of the Shandong Cenozoic alkali basalts. Niu [2005] suggested that the Cenozoic basalts in eastern China are the product of decompressional melting of the eastward flat flow of the asthenosphere, which had been metasomatized by low-degree melts. Liu *et al.* [2008], Chen *et al.* [2009], and Zeng *et al.* [2011] stressed the role of the delaminated or subducted mafic lower continental crust, which experienced an early melting event at the rutile stability field before incorporation into basaltic mantle sources. In recent years,

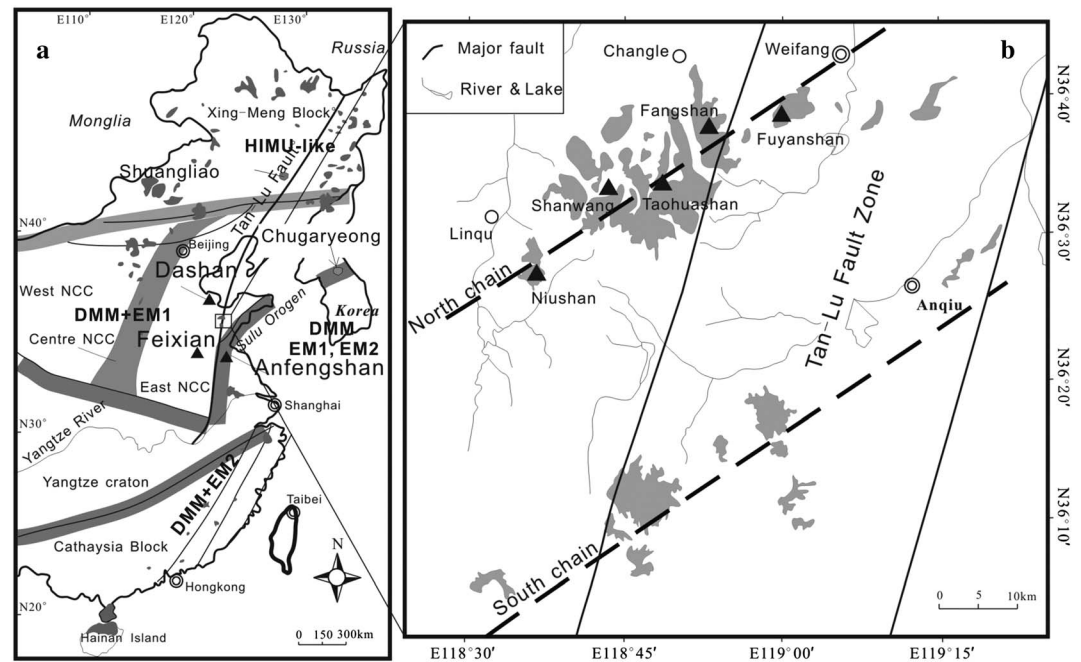


**Figure 1.** (a) Simplified geological map of eastern China. The marked mantle types are from Zou *et al.* [2000], Choi *et al.* [2005], and Y. G. Xu *et al.* [2012]. (b) Distribution of the Cenozoic chain-forming volcanoes in Shandong. Dashed lines show the northern and southern volcanic chains. Black triangles indicate the volcanoes in the north chain studied by Zeng *et al.* [2011]. This map was simplified and modified after Zeng *et al.* [2011].

the role of oceanic crust, specifically the subducted Pacific oceanic crust, has been increasingly suggested [Y. G. Xu *et al.*, 2012; Z. Xu *et al.*, 2012, 2014; Sakuyama *et al.*, 2013]. For example, Z. Xu *et al.* [2012] proposed that the Shandong Cenozoic basalts were derived from the lithospheric mantle, which had been hybridized by melts derived from the subducted Pacific slab and transformed from peridotite to pyroxenites [this model is the same as that proposed by J. J. Zhang *et al.* [2009] and Z. M. Zhang *et al.* [2009], for the Su-Wan Cenozoic basalts]. Sakuyama *et al.* [2013] suggested a more complex mantle source that contained contributions from the fluids released by the hydrated mantle transition zone and the partial melts from a carbonated oceanic crust. Similarly, the Cenozoic Chifeng continental flood basalts in eastern China (Figure 1), which are close to the position of the western edge of the stagnant Pacific slab within the mantle transition zone (MTZ) at the surface, were suggested to have been produced by slab-triggered wet upwelling from the hydrous MTZ [Wang *et al.*, 2015].

The  $H_2O/Ce$  does not become fractionated due to mantle partial melting and crystallization during magma evolution, and the  $H_2O/Ce$  ratio of magma could represent that of the mantle source [Dixon *et al.*, 2002; Michael, 1995]. Although it is often suggested that the subducted oceanic slab would become extensively dehydrated [Dixon *et al.*, 2002], there are several clues indicating that the subducted oceanic slab could maintain a high water content into the deep earth beyond the arc [Niu, 2005, and the references therein; Garth and Rietbrock, 2014; Savage, 2012], such as in the Manus basin, Southwest Pacific. There, the  $H_2O/Ce$  ratio ranges from 367 to 903 in submarine basaltic glasses, with low  $\delta D$  values from  $-100$  to  $-126$  and  $He^3/He^4$  ratios of 10 to 15  $R/R_A$ , which were attributed to an old, dehydrated oceanic slab [Shaw *et al.*, 2012]. While the mafic lower continental crust and the subducted continental eclogite are relatively dry, the corresponding  $H_2O/Ce$  ratios are low [Yang *et al.*, 2008; Katayama *et al.*, 2006; see the calculation in the following section]. Thus, the magma water contents ( $H_2O/Ce$  ratio) have the potential to distinguish between components from the subducted oceanic crust mentioned and other components. Chen *et al.* [2015] investigated the magma water contents of the Shuangliao basalts (51–42 Ma) in Northeast China, whose mantle source was suggested to contain recycled Pacific oceanic crust [Y. G. Xu *et al.*, 2012]. They found that the estimated magma water content varied from 0.9 to 3.09 wt.%, which overlaps with the range of island arc basalts [Plank *et al.*, 2013]. In fact, the model of metasomatism of depleted mantle by low-degree partial melts in the lithosphere-asthenosphere boundary involves intramantle fractionation controlled by high-temperature partitioning of elements between minerals and melts or fluids [Niu, 2005; Pilet *et al.*, 2008; Meng *et al.*, 2014], which would

not cause the oxygen isotope composition anomaly ( $\delta^{18}\text{O}$  deviated from the value of basalts from the normal mantle value) [Chiba *et al.*, 1989; Zheng, 1991; Eiler, 2001]. On the contrary, when the mantle source involved recycled continental or oceanic crust, which exhibits significantly different  $\delta^{18}\text{O}$  values than normal mantle [Eiler, 2001, and the references therein], the basalts would also exhibit the signature  $\delta^{18}\text{O}$  anomaly [Eiler *et al.*, 2000; Gurenko *et al.*, 2011].

In this work, we focus on the Fuyanshan volcano in the west field of the Shandong Cenozoic basalts. We examine the existing models mentioned above in the new view of magma water content and in situ oxygen isotope compositions of clinopyroxene (cpx) phenocrysts.

## 2. Geological and Sample Settings

The North China Craton (NCC), one of the oldest cratons in the world, is located in the central part of eastern China (Figure 1) and is composed of two Archean blocks (the Eastern Block and Western Block) and one Proterozoic orogen (the Central Zone) [G. C. Zhao *et al.*, 2005; Z. F. Zhao *et al.*, 2005]. At the south margin of the NCC lies the Dabie-Sulu orogen, which was formed by the subduction of the Yangtze block beneath the North China block in the Triassic and was separated into two terrains by approximately 500 km of left-lateral strike-slip displacement along the Tan-Lu fault. In the Eastern Block, the lithospheric mantle transformed from a typical cratonic mantle (cold, thick, and refractory) to a hot, thin, and fertile mantle during the late Cretaceous [Griffin *et al.*, 1998; Menzies *et al.*, 1993, 2007]. The seismic tomography demonstrates that the subducted Pacific slab is stagnant in the mantle transition zone beneath the east of China, and the heading edge is nearly under the Shandong Province [Fukao *et al.*, 1992; Huang and Zhao, 2006].

The field of alkali basalts in Shandong Province is part of the Cenozoic volcanic belt in the eastern part of the NCC and is near the Sulu-Dabie orogen (Figure 1). These basalts can be subdivided into two episodes [Luo *et al.*, 2009]. The first period of activity occurred from 24.0 to 10.3 Ma near the Tan-Lu fault zone, and the rocks are mainly alkaline basalts ranging from alkali olivine basalts to basanites. The activity of basalts in the second period occurred from 8.7 to 0.3 Ma and was scattered in the regions far from the Tan-Lu fault zone; their rocks are mainly basanites and nephelinites, such as the Dashan alkali basalts [Zeng *et al.*, 2010].

Zeng *et al.* [2011] investigated the genesis of the basalts from eight volcanoes belonging to the earlier episode (Figure 1). Petrologically, in these samples, olivine and/or cpx are the main phenocrysts, while the plagioclase (pl) always crystallized as microlites in matrix. The  $\text{SiO}_2$  contents vary from 43.20 to 47.62 wt.%, and the alkalis ( $\text{Na}_2\text{O} + \text{K}_2\text{O}$ ) vary from 3.68 to 5.53 wt.%. The bulk rocks have MgO in the range of 8.18 to 11.75 wt.%, Ni of 141 to 253 ppm, and Cr of 276 to 352 ppm, and the bulk rock Mg# values vary from 56 to 62 (all Fe was considered as  $\text{Fe}^{2+}$ ) (Data Set S1 of the supporting information). The high Cr content and lack of a Eu anomaly in all of these samples indicated that there was no significant amount of cpx and pl fractionated out from the magma to form cumulates. Significant crust assimilation was ruled out due to the lack of correlation between MgO and  $^{87}\text{Sr}/^{86}\text{Sr}$  [Zeng *et al.*, 2011]. All of these basalts have OIB-like trace element patterns, and their Sr-Nd isotopes vary from 0.7033 to 0.7040 and 0.5126 to 0.5129, respectively (Figure 2a). One important characteristic is the “decoupling” between  $\epsilon\text{Nd}$  and  $\epsilon\text{Hf}$ : with decreasing  $\epsilon\text{Nd}$ ,  $\epsilon\text{Hf}$  increasingly has higher values relative to the mantle array (Figure 2b). Zeng *et al.* [2011] suggested that this decoupling could be best explained by the involvement of recycled continental eclogites in the mantle source.

From these well-studied samples, we choose six from the Fuyanshan volcano to investigate their water contents and oxygen isotope compositions, because they have abundant cpx phenocrysts and span a large variation in trace element patterns and radiogenic isotopes (Figure 2). In addition, one sample from the nearby Niushan was analyzed for oxygen isotope composition.

## 3. Analytical Methods

It is challenging to measure the water content of continental basalts because, if it exists at all, quenched glass is typically scarce and seriously degassed in continental volcanoes. The melt inclusions in olivine are also scarce, and their small sizes also make them susceptible to hydrogen diffusion through the host mineral [Chen *et al.*, 2011; Gaetani *et al.*, 2012]. Based on the dependence of the water partition coefficient between cpx and basaltic melt ( $D^{\text{cpx/melt}}$ ) on the tetrahedral  $\text{Al}^{3+}$  in cpx, Wade *et al.* [2008] first suggested that the water content of magma could be recovered by the water content in the cpx phenocrysts and the

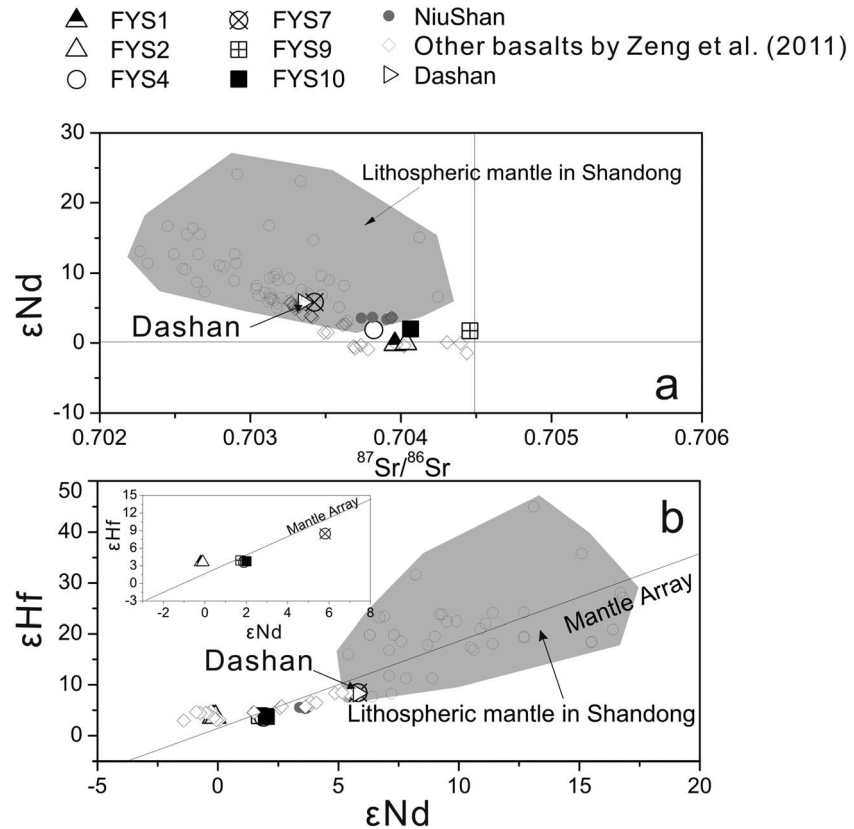


**Figure 2.** Sr-Nd-Hf isotope compositions of the Shandong basalts. The Sr-Nd-Hf isotopes of the lithospheric mantle are represented by the peridotite xenoliths from the Cenozoic basalts in Shanwang [Chu et al., 2009] and Beiyang [Xiao et al., 2010]. Primitive mantle values are from McDonough and Sun [1995]. The inset in Figure 2b represents the multiplication of the plot of Nd-Hf isotopes. The mantle array line is defined by:  $\epsilon_{Hf} = \epsilon_{Nd} * 1.59 + 1.28$  [Chauvel et al., 2008]. Data for the Shandong basalts are from Zeng et al. [2011]. Data for the Dashan basalts are from the supplement file of Zeng et al. [2011].

chemical composition. O'Leary et al. [2010] measured the  $D^{cpx/melt}$  for basaltic systems with very low and high  $Al_2O_3$  contents and refined the correlation between  $D^{cpx/melt}$  and the Al content of cpx to  $(\ln d_{H_2O}^{cpx/melt} = -4.2(\pm 0.2) + 6.5(\pm 0.5)X_{IVAl}^{cpx} - 1.0(\pm 0.2)X_{Ca}^{cpx})$ . The island arc basalt (Galunggung, Irazú, and Arenal volcano) recovered water contents predicted using this new equation that are identical or higher than those recovered from melt inclusions in olivine or cpx phenocrysts [O'Leary et al., 2010]. Xia et al. [2013] applied this approach to estimate the water content of Mesozoic picritic basalts with "arc-type" trace element patterns in the NCC. The estimated magma water content ( $3.4 \pm 0.7$  wt.%) is rather consistent with the average water content of global island arc basalts ( $3.9 \pm 0.4$  wt.%) [Plank et al., 2013]. These case studies indicate that a phenocryst-based approach could be used to successfully recover the water content of magma. Thus, in this work we use this method to estimate the water content of the Shandong alkali basalts. The detailed analytical procedure is the same as that used by Xia et al. [2013], Chen et al. [2015], and Liu et al. [2015], in which the water content of cpx phenocrysts was measured using Fourier transform infrared (FTIR) with an unpolarized beam.

### 3.1. FTIR Analysis

A polarized beam is preferred for measuring the water content in anisotropic minerals. However, this method requires cutting the minerals along three perpendicular directions, which is challenging for small cpx phenocrysts. The phenocrysts typically contain mineral/melt inclusions and cracks, and exhibit chemical composition zones, which largely reduce the likelihood of finding a sufficient region for FTIR analysis without interference due to hydrous minerals or water absorption. Additionally, the combined effects of crystallization, degassing, and diffusion during the magma evolution usually lead to various water contents in cpx phenocrysts

[Wade *et al.*, 2008; Nazzareni *et al.*, 2011], which makes it invalid to conduct unpolarized FTIR analyses on multiple randomly orientated cpx grains and to calculate the total absorption by three times the average absorption values for individual cpx grains [Sambridge *et al.*, 2008; Kovács *et al.*, 2008].

Xia *et al.* [2013] evaluated the deviation of absorption of one single unpolarized FTIR measurement on a randomly orientated cpx grain from the result of the classical polarized FTIR measurement ( $\text{Dev} = (3A^{\text{unp}}/A_{\text{total}} - 1) \times 100\%$ , where Dev is the deviation described above,  $A^{\text{unp}}$  is the integral unpolarized absorbance of a randomly oriented cpx grain, and  $A_{\text{total}}$  is the total absorbance, which is equal to the sum of the polarized absorbance along three principle optical axes). They found that for augitic to diopsidic cpx phenocrysts with OH bands, such as those of PMR-53 [Bell *et al.*, 1995, Figure 3], the largest deviation was 19%. However, Withers [2013] argued that Sambridge *et al.* [2008] and Kovács *et al.* [2008] adopted an inaccurate expression for calculating  $A_{\text{unp}}$  and thus underestimated the error of unpolarized measurements [see the "THEORY" section in Withers, 2013], which is the basis for Xia's error evaluation. Following the procedure of Xia *et al.* [2013; see the "Feasibility of unpolarized beam" section in Xia *et al.*, 2013], we adopted the accurate expression of unpolarized absorption [Withers, 2013, equations (11) and (14)] and the published polarized absorption along three principle optical axes [including the polarized spectra for synthesized and natural cpx, which can be found in Liu *et al.*, 2015] to calculate the deviation ( $\text{Dev} = (3A^{\text{unp}}/A_{\text{total}} - 1) \times 100\%$ ). The results indicate that all of the deviations are smaller than 20% [Liu *et al.*, 2015]. As an experimental test, we cut several cpx megacrysts (hosted by the Nushan basanite) with similar major elements and OH bands of cpx PMR-53 into cubes, which contain three random but mutually perpendicular surfaces. We found that three times of  $A^{\text{unp}}$  measured on each group of surfaces are also consistent with the total absorption obtained by polarized measurement ( $A_{\text{total}} = 1/2 \sum (A(\theta) + A(\theta + 1/2\pi))$ , where  $\theta$  is the angle between the direction of the electronic field of incident light and one specific principle optical axis) [Libowitzky and Rossman, 1996] within 20% differences [Liu *et al.*, 2015]. These tests confirm that for cpx with similar absorbance characteristics as PMR-53, the unpolarized measurement would not cause considerable uncertainty. Thus, in this work, we followed the method suggested by Xia *et al.* [2013] and Liu *et al.* [2015].

The unpolarized FTIR measurements were conducted at the CAS Key Laboratory of Crust-Mantle Materials and Environments of the University of Science and Technology of China (USTC) with a Nicolet 5700 FTIR spectrometer coupled with a Continuum microscope using a KBr beam splitter and equipped with a liquid-nitrogen-cooled MCT-A detector. The basalt samples were rendered into double-polished thin sections, with thicknesses ranging from 80 to 150  $\mu\text{m}$ . The light source and pathway were flushed with a purified air, which was free of  $\text{CO}_2$  and  $\text{H}_2\text{O}$ , as was the sample-holding cell. For each cpx grain, unpolarized spectra ranging from 1000 to 4500  $\text{cm}^{-1}$  were obtained using a total of 256 or 512 scans (depending on the cpx water content), with a resolution of 4  $\text{cm}^{-1}$ . A square light spot was used with dimensions ranging from 30 by 30  $\mu\text{m}$  to 100 by 100  $\mu\text{m}$ , depending on the size and quality of the mineral grain. The optically cleaned, inclusion, and crack-free areas were chosen for measurement. Profile analyses were conducted for a subset of cpx grains to examine H diffusion. A digital spiral micrometer was used to measure the thickness of each cpx grain (the average of the three measurements).

The modified Beer-Lambert law ( $c = A / (l \times t)$ ) was used to calculate the water content of cpx, in which  $A$  is the total absorption (here calculated as three times the unpolarized absorption),  $l$  is the absorption coefficient (7.09  $\text{ppm}^{-1} \text{cm}^{-2}$ ), and  $t$  is the thickness. This method could allow a calculation of cpx water contents with a maximum error of 30% [Xia *et al.*, 2013]. The water contents of the basaltic melts, from which the cpx phenocrysts crystallized, were calculated via the following steps: (1) calculate the water partition coefficient  $D_{\text{H}_2\text{O}}^{\text{cpx/melt}}$  based on the major element composition data (using Electron Micro-Probe Analysis (EMPA)) of cpx and In

$D_{\text{H}_2\text{O}}^{\text{cpx/melt}} = -4.2(\pm 0.2) + 6.5(\pm 0.5)X_{\text{IVAl}}^{\text{cpx}} - 1.0(\pm 0.2)X_{\text{Ca}}^{\text{cpx}}$  [O'Leary *et al.*, 2010]; (2) calculate the water content of the basaltic melt, based on the cpx water content (using FTIR) and the calculated  $D_{\text{H}_2\text{O}}^{\text{cpx/melt}}$  ( $C_{\text{H}_2\text{O}}^{\text{melt}} = C_{\text{H}_2\text{O}}^{\text{cpx}} / D_{\text{H}_2\text{O}}^{\text{cpx/melt}}$ ). The error of the calculated water content of a specific cpx in the melt equilibrium can be estimated using

$\sqrt{(\sigma C_{\text{cpx}}^{\text{water}})^2 + (\sigma D_{\text{water}}^{\text{cpx/melt}})^2}$ . When the maximum partition coefficient uncertainty is assumed to be 30%, the resulting maximum uncertainty of the calculated water content in the melt is 42%. Note that in Liu *et al.* [2015], this uncertainty may be underestimated by setting the  $\sigma D_{\text{water}}^{\text{cpx/melt}}$  to 10%.

### 3.2. Major and Trace Elemental Composition Analysis for Cpx Phenocrysts

The chemical compositions of these cpx phenocrysts and coexisting olivine phenocrysts were analyzed using a Shimadzu Electron Probe Microanalyzer (EMPA 1600) at the CAS Key Laboratory of Crust-Mantle Materials and Environments, USTC. The compositional homogeneities of cpx and olivine phenocrysts were ascertained using back-scattered electron (BSE) imaging. During the quantitative composition analyses, the operating conditions included a 15 kV acceleration voltage, a 20 nA beam current, and a  $<5\ \mu\text{m}$  beam diameter. Natural minerals and synthetic oxides were used as standards, and a program based on the ZAF [Armstrong, 1989] procedure was used for data correction. When analyzing the cpx phenocrysts, multipoint measurements were made within the FTIR analytical region. The olivine phenocryst analyses were performed in the cores.

The trace element compositions of several cpx phenocrysts from samples FYS07 and FYS10 were analyzed using laser ablation inductively coupled plasma-mass spectrometry LA-ICP-MS at the Key Laboratory of Continental Dynamics, Northwest University, Xi'an. The same sample blocks prepared for the secondary ion mass spectrometer (SIMS) analysis were used here. BCR-2, NIS610, and GSE-1 glass were used as standards. During the analysis session, analyses were conducted on standards after every five sample analyses.

### 3.3. Oxygen Isotope Analysis

A total of 8 to 10 cpx phenocryst grains from three Fuyanshan samples (FYS7, FYS9, and FYS10) and 5 from a Niushan sample were chosen for oxygen isotope analysis after the FTIR and electromagnetic pulse analyses. No OH bands of hydrous minerals and complex major element zones were found in these cpx grains. The ion microprobe analyses were conducted using a SIMS (Cameca IMS-1280) at CRPG-CNRS, Nancy. Four Nushan cpx megacrysts (NSH2, NSH5, NSH7, and NSH6), whose major element and oxygen isotope compositions were published by Xia *et al.* [2004] (see Data Set S2), were used as the standards to trace the "matrix effect." NSH6 was also measured to bracket the samples and monitor the possible instrumental drift. The Nushan cpx megacrysts have major element compositions similar to the cpx phenocrysts in the Shandong basalts.

A  $\sim 5\text{--}8\ \text{nA}$ , 10 kV Cs<sup>+</sup> primary ion beam with a spot size of approximately  $20\ \mu\text{m}$  was used. The sample charge was balanced using an electron flood gun. The primary beam and electron beam were carefully tuned at the beginning of each session, as well as for each sample mount. The secondary O<sup>-</sup> ions were accelerated at 10 kV and analyzed at a mass resolution power of 3000. The energy slit was set at 50 eV. Oxygen isotopes were measured in multicollection mode, using two off-axis Faraday cups: L2 for  $^{16}\text{O}$  and H1 for  $^{18}\text{O}$ . For each spot analysis, 60 s of presputtering,  $\sim 40\ \text{s}$  of automated centering, and 150 s of integrating oxygen isotope signals were conducted. The typical count rates for  $^{16}\text{O}^-$  were  $\sim 5 \times 10^9$  cps. The internal precision for one spot analysis was typically better than 0.1‰. For each cpx phenocryst, three points were chosen for analysis, and the measured values were independently corrected for matrix effects. For each cpx grain, the oxygen isotopes ( $\delta^{18}\text{O}$ ) were expressed as the average of these multiple analyses in the V-SMOW scale. The matrix effect was corrected according to the correlation between instrumental fractionation and the Mg# of cpx. The instrumental drift over time was calibrated using a linear function of time. The combined precision and accuracy for each cpx grain is  $\sim 0.5\text{‰}$ . The details of the calibration and accuracy assessment can be found in Text S1 in the supporting information.

## 4. Results

### 4.1. Chemical Compositions of Cpx and Ol Phenocrysts

The cpx phenocrysts are augitic to diopsidic, with Mg# values ranging from 71 to 83.4, and have Cr<sub>2</sub>O<sub>3</sub> contents varying from 0.1 to 0.3 wt.% (see Data Set S3). The BSE image shows that the cpx phenocrysts are nearly homogenous or display oscillatory zones (Figures 4a–4d). The olivine phenocrysts exhibit Mg# values ranging from 68 to 83, and their CaO contents are generally higher than 0.1 wt.% (Data Set S3). For each sample, the highest Mg# values in cpx are very close to those of olivine phenocrysts and are nearly in equilibrium with the bulk rock if the Fe-Mg exchange coefficient (Kd) is assumed to be  $0.33 \pm 0.03$  [Roeder and Emslie, 1970].

### 4.2. Water Content in Cpx and Equilibrated Melt

Representative unpolarized spectra for the Shandong cpx phenocrysts are shown in Figure 3. The IR absorption bands of the cpx grains can be subdivided into three groups:  $3630\text{--}3620\ \text{cm}^{-1}$ ,  $3540\text{--}3520\ \text{cm}^{-1}$ ,

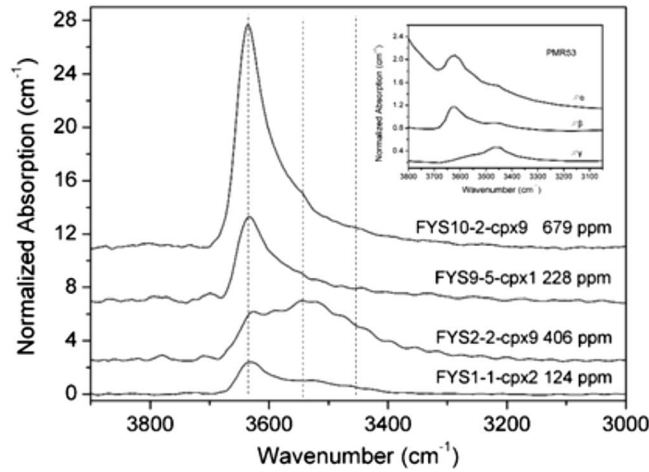


**Figure 3.** Representative IR spectra of the cpx phenocrysts in the Fuyanshan (FYS) alkali basalts. The spectra have been normalized to a thickness of 1 cm, and the baseline has been corrected. The numbers show the water contents of that cpx grain by the method suggested by Xia *et al.* [2013]. The insert shows atypical OH absorption band along three main extinction axes for the cpx PMR53 [Bell *et al.*, 1995]. Dashed lines show the corresponding OH bands in clinopyroxene grains.

content calculations using the unpolarized FTIR measurements [Sambridge *et al.*, 2008; Kovács *et al.*, 2008; Férot and Bolfan-Casanova, 2012; Xia *et al.*, 2013; Withers, 2013]. The FTIR profile analysis shows that most of the cpx grains exhibit homogeneous H<sub>2</sub>O contents or H<sub>2</sub>O-poor thin rims (in the region within the outermost 50 μm) (Figure 4),

and 3470–3450 cm<sup>-1</sup>. The positions of the absorption bands are similar to those reported in previous studies of both natural and experimental minerals, and have been correlated with the vibrations of structural OH [Skogby and Rossman, 1989; Skogby *et al.*, 1990; Bell and Rossman, 1992; Ingrin and Skogby, 2000; Grant *et al.*, 2007; Yang *et al.*, 2008; Peslier *et al.*, 2002; Sundvall and Stalder, 2011; Hao *et al.*, 2012; Mosenfelder and Rossman, 2013; Doucet *et al.*, 2014]. Additionally, these bands are similar to the bands from the cpx phenocrysts in the Feixian basalts, for which the feasibility of unpolarized FTIR was described [Xia *et al.*, 2013]. The linear absorption intensity (the height of one specific OH band) is always less than 0.3 (not shown), confirming that the OH in these cpx phenocrysts is weakly absorbed, which allows for quantitative water content

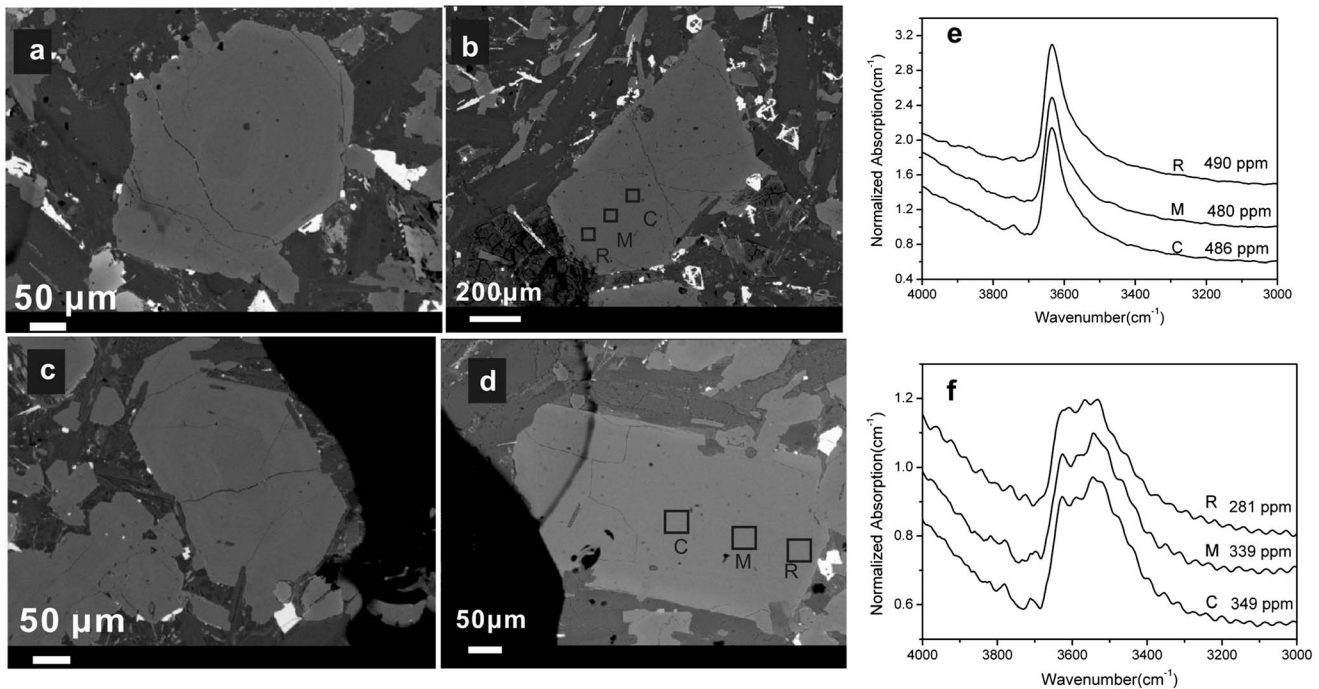


**Figure 4.** BSE images of the clinopyroxene phenocrysts in the Shandong basalts and the typical FTIR absorption profiles. Figures 4a and 4c show cpx phenocrysts with oscillation zones; Figures 4b and 4d show cpx phenocrysts with homogeneous zones. Figures 4e and 4f show the two examples of profile analyses for cpx in sample FYS10. The black squares show the positions of spots for FTIR analysis, with dimensions of 30 μm on each side. Their corresponding IR spectra are shown in Figures 4b and 4d, respectively. The absorption intensity has been normalized to 1 cm. The labels C, M, and R indicate the core, mantle, and rim zones of phenocrysts, respectively. The numerical values presented with each spectrum are the calculated water content. Note that the water content of cpx in Figure 4a are nearly homogeneous, whereas the grains in Figure 4c show thin low-water-content rims, which would be caused by diffusion.

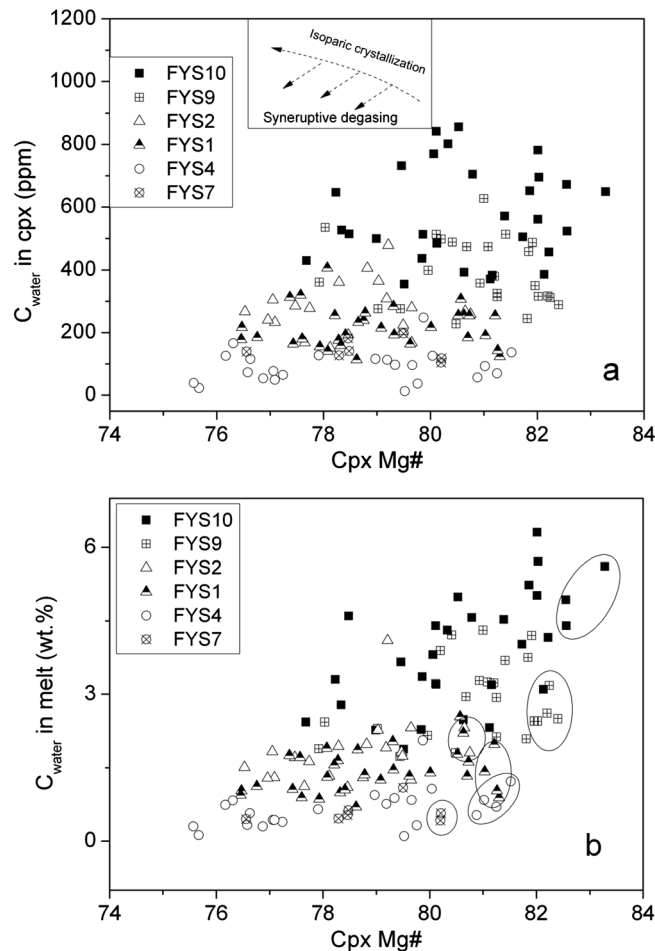


**Figure 5.** The water content of the cpx phenocrysts and the melt vs. Mg# of the cpx phenocrysts in the Fuyanshan basalts. (a) Water contents of the cpx phenocrysts from Fuyanshan (sample FYS); the insert is a schematic drawing of the change in water content associated with crystallization and syneruptive degassing during magma evolution. (b) The circles mark the cpx grains with the highest Mg# used to calculate the water content of the melt.

cpx phenocrysts are listed in Data Set S4, in analytical chronological order. The matrix effect corrected  $\delta^{18}\text{O}$  values are listed in Table 1. Figure 6 illustrates the cpx phenocryst  $\delta^{18}\text{O}$  values and their associated Mg# values. Several characteristics can be identified: (1) the cpx  $\delta^{18}\text{O}$  values in the Shandong basalts straddle the value of normal mantle-derived cpx ( $5.6 \pm 0.2\text{‰}$ ) [Eiler, 2001; Matthey et al., 1994], ranging from 3.6‰ to 6.4‰, but with most lower than  $5.6 \pm 0.2\text{‰}$ ; (2) the majority of the cpx  $\delta^{18}\text{O}$  values in the Niushan sample are slightly lower than  $5.6 \pm 0.2\text{‰}$  and remain nearly constant with decreasing Mg#; (3) the cpx  $\delta^{18}\text{O}$  values from the FYS samples span a wide range within a small Mg# variation, especially for the cpx with Mg# values close to 80; and (4) a rough correlation between Mg# and  $\delta^{18}\text{O}$  could be identified in sample FYS7.

## 5. Discussion

### 5.1. Origin of the Heterogeneous $\delta^{18}\text{O}$

As plotted in Figure 6, most of the analyzed cpx phenocrysts exhibit  $\delta^{18}\text{O}$  values lower than the cpx values from the majority of the mantle peridotites or the normal mantle-derived basalts [Eiler, 2001; Matthey et al., 1994]. In addition, the cpx in samples FYS7 and FYS10 spans large intervals, ranging from  $\sim 2.5\text{‰}$  to  $\sim 1.5\text{‰}$ , respectively.

These variable  $\delta^{18}\text{O}_{\text{cpx}}$  values could not have been caused by partial melting, fractional crystallization, and devolatilization, given the consensus that all of these processes lead to an oxygen isotope fractionation within 0.1‰ for basaltic melts, with MgO contents between 8 and 3 wt.% [Eiler, 2001, and the references therein].

ruling out significant water loss by diffusion during ascent. The calculated water contents of the cpx phenocrysts are plotted with their Mg# values in Figure 5a. The cpx phenocryst water contents range from 13 to 802 ppm by weight, which belie the analytical uncertainty (<30%). However, the water contents of cpx for each sample are systematically different (Figure 5a). The calculated water contents in the equilibrium melts with specific cpx also vary substantially (Figure 5b, see the Data Set S3), ranging from 0.1 to 6.3 wt.%, with most being higher than 0.5 wt.%. In addition, the water contents of the equilibrium melts with the cpx phenocrysts decrease as the largest Mg# values in each sample decrease (the cpx marked by the ellipse in Figure 5b), which appears consistent with the degassing process during fractional crystallization. However, further discussion will exclude this possibility.

### 4.3. Oxygen Isotope Compositions of Cpx Phenocrysts

In the context of Mg#, most of the cpx samples are chemically bracketed by the standards. Very few parts of the FYS cpx exhibit higher Mg# values than the standards. The raw analytical results of the standard Nushan cpx megacryst (NSH6) and the Shandong

**Table 1.** The Oxygen Isotope Composition of Cpx Phenocrysts in the Fuyanshan Basalts<sup>a</sup>

	Grain	Mg#	Averaged Measured $\delta^{18}\text{O}$	IMF	Averaged Corrected $\delta^{18}\text{O}$	1SE
FYS07	FYS07-5-cpx5	79.84	-16.64	-20.94	4.09	0.35
	FYS07-5-cpxa	77.3	-17.11	-21.07	3.59	0.17
	FYS07-5-cpxb	78.98	-17.06	-21.4	4.07	0.19
	FYS07-1-cpx3	79.28	-15.96	-21.79	5.64	0.06
	FYS07-15-cpx1	82.05	-15.75	-22	6.12	0.27
	FYS07-a	79.97	-15.8	-22.35	6.34	0.35
	FYS07-b	80.21	-16.28	-22.22	5.74	0.18
	FYS07-d	80.12	-16.77	-22.08	5.11	0.06
FYS09	FYS09-4-cpx7	80.23	-16.92	-22.2	5.33	0.04
	FYS09-3-cpax	80	-6.63	-11.39	4.5	0.21
	FYS09-3-cpx5	81.91	-6.19	-11.33	5.05	0.1
	FYS09-5-cpx4	80.5	-4.91	-11.13	6.04	0.16
	FYS09-5-a	81.91	-5.37	-11.21	5.75	0.15
	FYS09-5-c	74.98	-6.37	-11.28	4.36	0.17
	FYS09-d	80.71	-5.44	-11.49	5.88	0.02
	FYS10	FYS10-4-cpx4	79.7	-16.84	-21.47	4.41
FYS10-4-cpx4b		80.2	-16.73	-21.71	4.85	0.16
FYS10-4-cpx8		80.86	-16.91	-22.28	5.22	0.07
FYS10-1-cpx9		81.3	-14.67	-20.64	5.84	0.05
FYS10-2-cpx6		80.4	-17.83	-22.65	4.77	-
FYS10-b		82.12	-17.37	-22.49	5.07	0.1
FYS10-b2		80.55	-14.24	-22.45	5.36	-
NiuS		NiuS3-3-cpx1c	79.11	-16.37	-21.6	4.97
	NiuS3-3-cpx1r	74	-15.55	-21.47	5.35	0.44
	NiuS3-3-cpx2	79.4	-15.9	-21.35	5.23	0.13
	NiuS3-3-Al	72.67	-14.83	-21.22	5.73	0.13
	NiuS3-3-cpx4	76.57	-16.01	-21.21	5.3	0.44

<sup>a</sup>“-” represents that the data just involved one measurement. SE is the standard error of the mean.

The possible causes include the following: (1) the artifact from IMF (Instrumental Fractionation Factor) correction; (2) the post-eruption secondary alteration; (3) the involvement of crustal materials with  $\delta^{18}\text{O}$  anomalies during magma transport, or interactions with meteorite water in the magma chamber; and (4)  $\delta^{18}\text{O}$  heterogeneities in the mantle source.

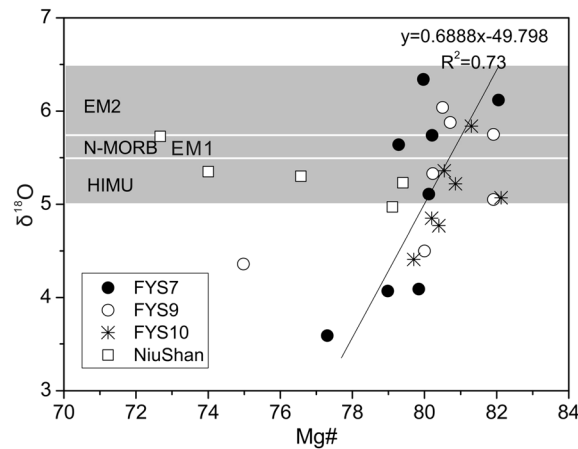


**Figure 6.** The oxygen isotope compositions of the cpx phenocrysts in the Shandong basalts. The range of  $\delta^{18}\text{O}$  values of cpx phenocrysts from the N-MORB, EM, and HIMU basalts, calculated from their published  $\delta^{18}\text{O}$  values of olivine phenocrysts [Eiler *et al.*, 1997; Widom and Farquhar, 2003] and the equilibrium fractionation between cpx and ol of 0.4‰, are also marked by the gray bars or double arrows. For sample FYS07, the linear least square fitting equation is shown.

The first possibility is not valid because the cpx phenocrysts in the Niushan sample exhibit similar  $\delta^{18}\text{O}$  values when their Mg# values span a larger range than the Mg# interval (from 80 to 72) (Figure 6). The post-eruption alteration process was also not responsible for the dominantly low  $\delta^{18}\text{O}$  values in the phenocrysts, given that all of the regions analyzed by SIMS were chosen after FTIR detection and the cpx  $\delta^{18}\text{O}$  are not dependent on the cracks and grain sizes (Figure 7). Although some of the granitoids, granitic gneisses, and eclogites in the Sulu orogenic belt exhibit low  $\delta^{18}\text{O}$  values [see review by Zheng *et al.*, 2003], they are highly enriched in  $^{87}\text{Sr}/^{86}\text{Sr}$ , are depleted in  $^{143}\text{Nd}/^{144}\text{Nd}$ , and have Nb-Ta-depleted and Pb-enriched trace element patterns [Jahn, 1998; Huang *et al.*, 2006; Tang *et al.*, 2008], which are in contrast with the relatively depleted Sr

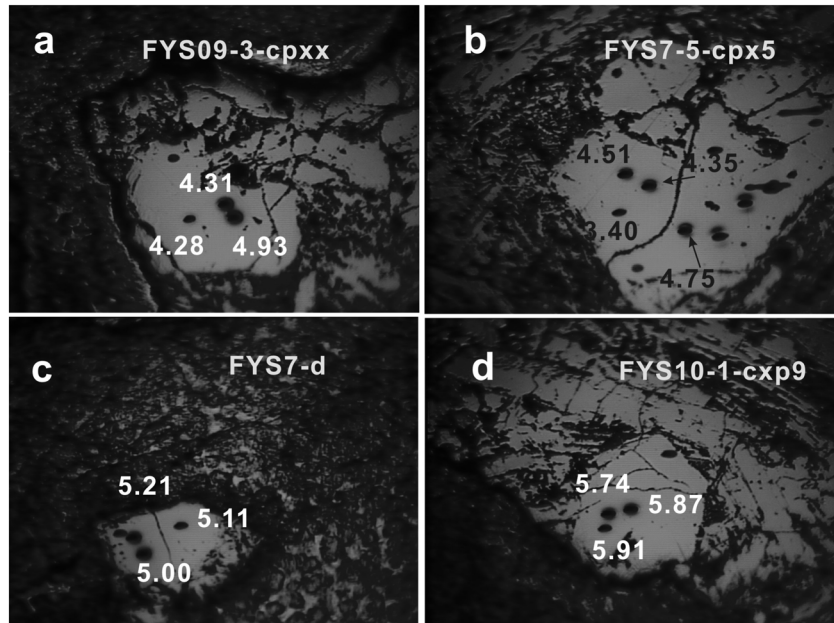


**Figure 7.** The in situ  $\delta^{18}\text{O}$  values of the cpx phenocrysts in the Shandong alkali basalts. The dark pits are the SIMS analysis points. The photos were collected by the Cameca 1280 automatically, and the horizontal length of each image is 1000  $\mu\text{m}$ . All data are IMF corrected.

isotopes and obvious OIB-like trace element patterns of the Shandong basalts. For instance, FYS07 contains cpx with  $\delta^{18}\text{O}$  values lower than the Niushan sample (Figure 6). However, the bulk rock data show that FYS07 has an MgO of 10.7 wt.%, lower  $^{87}\text{Sr}/^{86}\text{Sr}$  ratios, and higher  $^{143}\text{Nd}/^{144}\text{Nd}$  ratios than the Niushan cpx [Zeng *et al.*, 2011], which do not support crustal assimilation as an explanation for the observed  $\delta^{18}\text{O}$  anomaly. In addition, the euhedral shapes and chemical compositions of the analyzed cpx exclude the possibility that they were derived from crustal xenocrysts. Although the magma interactions with meteoritic water during the ascent would also lower the  $\delta^{18}\text{O}$  of the magma, and thus of the cpx phenocrysts, it is difficult to explain the simultaneous occurrences of  $\delta^{18}\text{O}$  values that are both higher and lower than the normal mantle value for the cpx, with an Mg# close to 80 (Figure 6). On the other hand, the calculation of the water-rock ratios in need to reduce the  $\delta^{18}\text{O}$  by 2.5‰ (FYS07) based on the following equation [Taylor, 1974]:

$$\frac{W}{R} = \frac{\delta^{18}\text{O}_R^f - \delta^{18}\text{O}_R^i}{\delta^{18}\text{O}_W^i - (\delta^{18}\text{O}_R^f - \Delta^{18}\text{O}_{RW})} \cdot \frac{C^i\text{O}_R}{C^i\text{O}_W} \quad (1)$$

where  $W/R$  is water-rock ratio by weight, superscript “ $f$ ” means final, “ $i$ ” means initial,  $C^i$  is the weight percentage of oxygen in rock or water,  $\delta^{18}\text{O}_W^i$  is assumed to be  $-7\text{‰}$ , and  $\Delta^{18}\text{O}_{RW}$  is calculated by  $1000\ln\alpha_{\text{basalt-water}} = 4.235 \times 10^6/T^2 - 7.912 \times 10^3/T + 2.54$  at  $1100^\circ\text{C}$  [Zhao and Zheng, 2003], shows that at least  $\sim 8$  wt.% meteorite water was required to interact with the magma. As shown in Figure 5, the low  $\delta^{18}\text{O}$  first occur for cpx with an Mg# value of 82, which means that meteorite water would likely penetrate into the lower continental crust. In reality, it is difficult for meteorite water to penetrate the lower continental crust.

Thus, it can be concluded that the various  $\delta^{18}\text{O}$  values of the cpx phenocrysts in the Shandong alkali basalts are not caused by an artifact of IMF correction, crustal contamination, or water-rock interaction, and they were likely inherited from mantle-derived magma(s). In fact, these  $\delta^{18}\text{O}$  signatures are consistent with the results for olivine and cpx phenocrysts from the Changle alkali basalts (obtained by laser fluorination method) [Z. Xu *et al.*, 2012]. Similar to the large  $\delta^{18}\text{O}$  variations identified in this study, Gurenko *et al.* [2011] reported the oxygen isotopic compositions of olivine phenocrysts from the Canary island basalts (La Gomera) using a SIMS analysis. Their results ranged from 1.7‰ with an Mg# close to 87 and 1.0‰ with an Mg# close to 90. The author explained the  $\delta^{18}\text{O}$  heterogeneities as being due to variable decompression melting of a high  $\mu$  (HIMU)-type mantle containing a recycled mid-ocean ridge basalt (MORB)-type oceanic crust in the form of reacted pyroxenite mixed with enriched mantle EM-type peridotite components. The specific process

**Table 2.** Calculated Average Water Contents in Fuyanshan Basalts<sup>a</sup>

Sample	Mg# > 80			Mg# > 75			Cw.melt (wt.%) Calculated From the Cpx With Highest Water Concentration	Highest Cw.melt (wt.%) in Each Sample
	Cw.melt (wt.%)	N	STD	Cw.melt (wt.%)	N	STD		
FYS01	1.6	11	0.47	1.4	29	0.46	1.90	2.54
FYS02	2.07	2	0.26	2.16	27	0.91	4.10	4.10
FYS04	0.87	5	0.25	0.67	23	0.42	2.06	2.00
FYS07	0.48	2	0.06	0.58	7	0.22	1.09	1.09
FYS09	3.11	20	0.72	2.98	27	0.84	4.31	5.00
FYS10	4.31	20	1.04	3.89	29	1.16	4.99	6.31

<sup>a</sup>N, the number of cpx grain involved in calculation; STD, the standard deviation.

was suggested as the crystallization of magmas with different  $\delta^{18}\text{O}$  produced phenocrysts with variable  $\delta^{18}\text{O}$ . They were stored in the magma plumbing system. Then, the subsequent magma batches engulfed such crystals and the melts, and carried them to the surface. A similar scenario was suggested for the low  $\delta^{18}\text{O}$  of plagioclase phenocrysts ( $4.5 \pm 0.4\text{‰}$  to  $5.5 \pm 0.3\text{‰}$ ) in the Borgarhraun flow in northern Iceland [Winpenny and MacLennan, 2014], as well as for the decreasing  $\delta^{18}\text{O}$  values as Mg# decreased in cpx phenocrysts from the Taihang basalts of China [Liu et al., 2015]. For the FYS samples, the  $\delta^{18}\text{O}$  heterogeneity in the cpx phenocrysts can also be explained by the process described above.

## 5.2. H<sub>2</sub>O Content of the Magma

### 5.2.1. Recovery of the Magma Water Content

We tested two strategies for recovering the magma water content. First, we calculated the average meltwater content for each sample (average of all points for each sample in Figure 5b) to estimate the magma water content. This was based on the following considerations: (1) Cpx phenocryst hybrids from distinct sources may occur, at least for samples FYS10, FYS9, and FYS7. Thus, the observed scatter in water contents (Figure 5b) would also be partly attributed to the mixing among melts with different water contents. And (2) an almost flat trend exists between the calculated water in the melt and the Mg# of cpx within the observed range of Mg# (75.5–83.3). This approach is consistent with Chen et al. [2015] and Liu et al. [2015], which used the averages of the meltwater contents derived from the cpx phenocrysts with Mg# > 75. Alternatively, the water content of the magma was calculated based on several cpx phenocrysts with the highest Mg# values (designated with ellipses in Figure 5b), which were used to estimate the water contents of the Feixian basalts by Xia et al. [2013]. The assigned magma water contents based on these two approaches are listed in Table 2.

To apply the first approach, we must assume that the proportion of the cpx in each sample could represent the proportion of melt involved in the mixing. Although this assumption may introduce additional uncertainty, it seems to be a reasonable and practical approach to compare the relative “humidity” of the magmas,

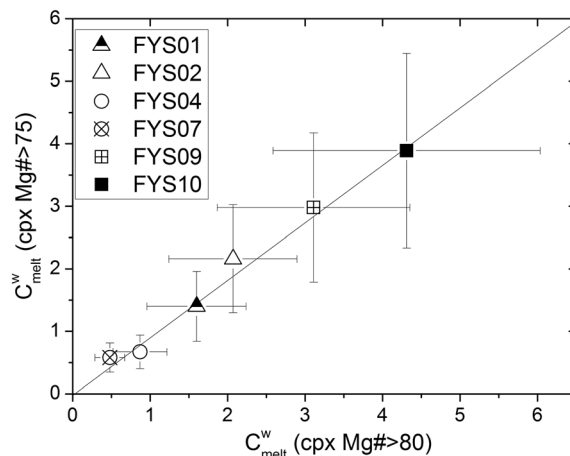


**Figure 8.** Comparison of assigned water content in magma for the FYS basalts. The error bar shows the relative error of 42%.

given that the FYS magmas do contain a mixture of melts/crystals with different geochemical characteristic (various  $\delta^{18}\text{O}$ ), which means that the geochemical data like major and trace elements, and radiogenic isotopic compositions obtained from bulk rock are also “mixed.” In fact, a comparison of the water contents calculated using these two approaches demonstrates that (Figure 8) the averages of all cpx and of the cpx with the highest Mg# values are relatively consistent. Considering the mixed nature of the cpx phenocrysts in our samples, we suggest that the water contents based on averaging all of the cpx grains are more reasonable. Because the relative standard deviation of the mean (Table 2) is smaller than the declared

uncertainty of each calculated meltwater content, the declared uncertainty (~42%) can be considered a maximum error of the average magma water contents. In the following discussion, these average water contents will be referred to as the “magma water content.”

### 5.2.2. The Cause for Variable Water Content Among Samples

The magma water contents of the Fuyanshan basalts span a wide range, from  $0.58 \pm 0.22$  (1SE) wt.% to  $3.89 \pm 1.16$  (1SE) wt.% (Table 2). It is necessary to explore whether these variations could have resulted from magma processes, including (1) mineral crystallization, (2) the diffusion of water from the cpx phenocrysts, (3) degassing during magma evolution, (4) crustal assimilation, and (5) the degree of partial melting.

The water content profile analyses of the cpx with both low and high water contents (Figures 4e and 4f) show that water concentrations in these cpx are relatively homogenous, except for the extreme outer rim. Both the highest and average water contents of cpx in each sample negatively correlate with Nb/U and positively correlate with  $^{87}\text{Sr}/^{86}\text{Sr}$  and heavy rare earth element (HREE) (only the relationship with Lu is shown) (Figure 9). These observations indicate that water in cpx phenocrysts, at least at the core, was not reset by diffusion. Degassing during magma ascent is also insignificant, due to two observations: (1) as shown in Figure 5b, for all samples the calculated water contents in melt equilibrium with the specific cpx phenocrysts do not decrease with decreasing Mg#, and the water concentration in cpx phenocrysts does not show significant heterogeneity, which would be expected if degassing occurs [Wade *et al.*, 2008]; and (2) the calculated water contents in magmas are also positively correlated with HREE (Figure 10) and  $^{87}\text{Sr}/^{86}\text{Sr}$  ratios, and negatively correlated with Nb/U ratios, similar to the correlations shown in Figure 9. In addition, fractional crystallization could not have been the main reason for the large magma water content variations because the recovered magma water contents do not correlate with the bulk MgO contents (Figure 11a). The assimilation of continental crust materials would also play an insignificant role in this process (see the description of the samples in section 2). Furthermore, the magma water contents are not correlated with (La/Yb)<sub>n</sub> (Figure 11b), indicating that the degree of partial melting is not a predominant factor.

Thus, the main reasons for the large variation of the water content of magma would be linked to their original characteristics and caused by various contributions of a water-rich magma.

## 5.3. Implications for the Mantle Source of the Shandong Basalts

### 5.3.1. Constraints From In Situ Oxygen Isotopes

Based on the decoupling of  $\epsilon\text{Hf}$  and  $\epsilon\text{Nd}$  relative to the mantle array line (Figure 2b), Zeng *et al.* [2011] suggested the Shandong basalts could be formed by mixing of two kinds of magmas. One is of relatively low  $^{87}\text{Sr}/^{86}\text{Sr}$  and high  $\epsilon\text{Nd}$  ( $^{87}\text{Sr}/^{86}\text{Sr} = 0.703351$ ,  $\epsilon\text{Hf} = +8.33$ ), but very enriched in LREEs, Nb, and Ta, which is represented by the Dashan nephelinites [Zeng *et al.*, 2011]. This was explained as the production of partial melting of a carbonated peridotite. The second, with a high  $^{87}\text{Sr}/^{86}\text{Sr}$  and low  $\epsilon\text{Nd}$ , is the melt from the residual fragments of the eclogites in Sulu orogeny, which were subducted into the upper mantle by the South China block [Wang *et al.*, 2009; Qiu *et al.*, 2006]. To explain the decoupling of  $\epsilon\text{Hf}$  and  $\epsilon\text{Nd}$  for the low  $\epsilon\text{Nd}$  samples (Figure 2b), Zeng *et al.* [2011] assumed a two-stage evolution model. In the first stage, the recycled Sulu eclogites (subducted into the deep mantle at 220 Ma) melted at 130 Ma to a degree of 55% to 60%, which caused a larger fractionation of Lu/Hf between residual and melt than that of Sm/Nd because of the garnet control during melting. These residuals finally melted upon mantle upwelling at 20 Ma, which was due to the flat eastward flow of the asthenosphere.

This model can successfully explain the radiogenic isotopes (the alternative explanation will be discussed in section 5.3.3), but it fails to explain the low  $\delta^{18}\text{O}$  obtained in this study. According to the model of Zeng *et al.* [2011], sample FYS7 should exhibit similar characteristics as the Dashan end-member (Figure 12), while FYS10 should exhibit a greater component of the residual eclogite (Figure 12). However, as shown in Figure 5, the majority of the cpx phenocrysts in both FYS7 and FYS10 have  $\delta^{18}\text{O}$  values lower than the normal mantle cpx ( $\sim 5.6 \pm 0.2\text{‰}$ , calculated from  $\delta^{18}\text{O}$  of olivine,  $5.2 \pm 0.2\text{‰}$ , and  $\Delta^{18}\text{O}_{\text{cpx-ol}} = 0.4\text{‰}$ ; Matthey *et al.*, 1994). On one hand, the occurrence of low  $\delta^{18}\text{O}$  (down to  $3.5\text{‰}$ ) in FYS7 cpx phenocrysts is not consistent with the relatively high  $\delta^{18}\text{O}$  for the carbonatites ( $5.5\text{‰}$  to  $12.7\text{‰}$ ) [Nelson *et al.*, 1988]. Thus, it does not support the theory that the Dashan end-member mantle is related to carbonatic metasomatism. On the other hand, although the eclogite in the CCSD (Chinese Continental Scientific Drilling) main hole exhibits  $\delta^{18}\text{O}$  values as low as  $-8.0\text{‰}$ , the main body of the eclogite yields  $\delta^{18}\text{O}$  values higher than  $4\text{‰}$  [Chen *et al.*, 2007a, 2007b]. Due to the high initial  $^{87}\text{Sr}/^{86}\text{Sr}$  ratios, which range from 0.706 to 0.710 even at 220 Ma, and obvious

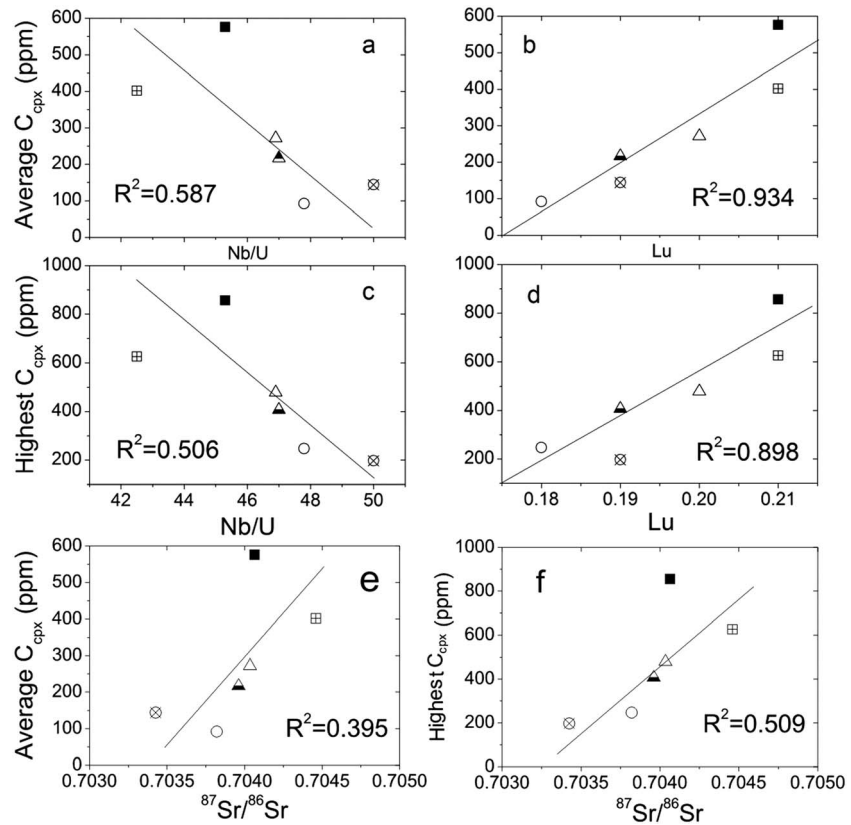


**Figure 9.** Comparison of water content in cpx phenocrysts with Lu concentration, Nb/U ratio, and <sup>87</sup>Sr/<sup>86</sup>Sr ratio of the bulk rock.

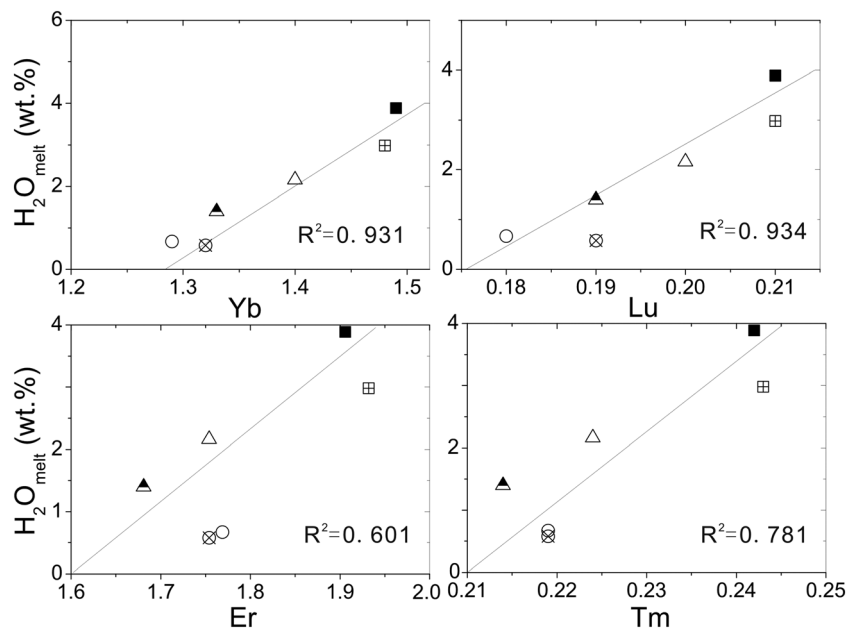


**Figure 10.** The comparison of calculated magma water contents (using approach one, average value) with HREE bulk rock concentrations. The relative analytical uncertainty is 42% for water and 10% for HREE, which is not plotted for clarity. An *F* test of the H<sub>2</sub>O vs. Yb regression indicates that the *F* value is 12.5, which is larger than the critical *F*(1, 4) = 7.71 at  $\alpha = 0.05$ . This means that although the uncertainty is large, the regression is significant at a 5% significance level. The HREE data of basalts are from Zeng *et al.* [2011].

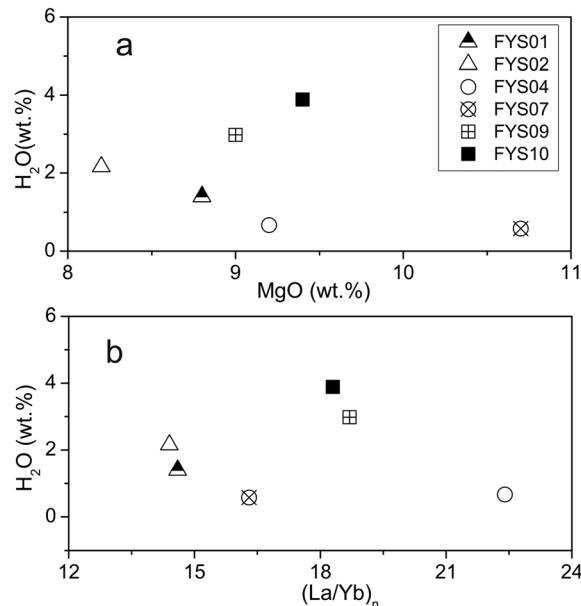


**Figure 11.** The variations of  $\epsilon_{\text{Hf}}$  and Lu/Hf ratios for the Shandong basalts. The gray symbols are for other samples than FYS in Zeng et al. [2011]. The dark long arrowed lines show the mixing trend and partial melting trend; for the detailed explanation see the main text.

geological observations. On one hand, seismic topography imaging illustrated that the subducted Pacific slab currently lies in the mantle transition zone beneath NCC at the present [Fukao et al., 1992; Huang and Zhao, 2006]; on the other hand, the pyroxenite xenoliths with low  $\delta^{18}\text{O}$  values (bulk rock 4.9–5.1‰), which were transformed from the remnants of lower oceanic crust, have been found in the subcontinental lithospheric mantle in Jiaohe, Northeast China [Yu et al., 2010]. In addition, the involvement of components from the Pacific oceanic crust is also supported by the spatial and temporal relationships among the geochemical characteristic of basalts and the subducting slab. Sakuyama et al. [2013] found that the late Cenozoic basalts in Shandong, with bulk FeO > 13 wt.% (total iron), were located directly above the western leading edge of the stagnant Pacific slab. Z. Xu et al. [2014] identified that the Eu/Eu\* and  $^{87}\text{Sr}/^{86}\text{Sr}$  of the 90–40 Ma magmas in North and Northeast China increase and decrease with decreasing emplacement age repetitively, mirroring a change of recycled oceanic components from the upper to lower parts of the subducted oceanic crust in the mantle source of basalts.

**5.3.2. Constraints From Water Content of Magma**

The highest calculated magma water content from the Shandong basalts (Table 2) is  $3.89 \pm 1.16$  wt.% (FYS10), which exceeds the normal water content range for mid-ocean ridge basalts (MORBs, <0.1 wt.%), ocean island basalts (OIBs, 0.3–1 wt.%), and back-arc basin basalts (0.2–2 wt.%), reaching the range of arc basalts (2–8 wt.%) [Dixon et al., 2004]. Such high water content suggests that the mantle source of the Shandong basalts contained a “wet” component.

**5.3.2.1. Mantle Components Other Than the Residual Sulu Eclogite**

It has been widely accepted that H<sub>2</sub>O/Ce ratio will not fractionate during the partial melting and crystallization of basaltic magma

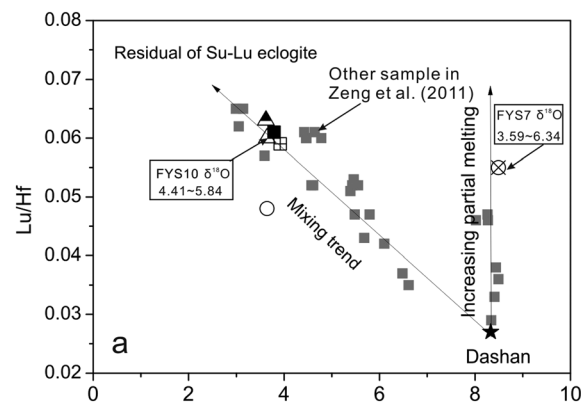


**Figure 12.** The comparison of the calculated water content and the bulk rock MgO and the primitive mantle normalized La/Yb ratios. The data sources are from Zeng et al. [2011].

**Table 3.** Comparison of H<sub>2</sub>O/Ce Ratios of the Magma Calculated From Different Approaches<sup>a</sup>

Sample	Cw.melt (wt.%)	Bulk Ce (ppm)	H <sub>2</sub> O/Ce <sup>1</sup>	Cpx Grain	C <sub>H2O</sub> Cpx (ppm)	C <sub>Ce</sub> Cpx (ppm)	D <sub>Ce</sub> <sup>2</sup>	D <sub>H2O</sub> <sup>3</sup>	H <sub>2</sub> O/Ce <sup>4</sup>	
FYS01	1.40	41	339							
FYS02	2.16	43	499							
FYS04	0.67	59	113							
FYS07	0.58	45	129							
				FYS7-15-cpx1	104	6.3	0.16	0.025	105	
				FYS7-1-cpx3	118	9.3	0.14	0.021	86	
									Average	96
FYS09	2.98	57	526							
FYS10	3.89	56	696							
				FYS10-2-cpx6	652	10.7	0.14	0.012	681	
				FYS10-2-cpx3	386	9.1	0.14	0.012	478	
				FYS10-4-cpx8	770	11.9	0.17	0.020	546	
				FYS10-4-cpx4	802	13.4	0.17	0.019	546	
				FYS10-1-cpx3	513	16.2	0.16	0.015	333	
				FYS10-3-cpx4	705	13.0	0.16	0.011	787	
				FYS10-1-cpx9	457	9.1	0.14	0.015	456	
									Average	547

<sup>a</sup>1, H<sub>2</sub>O/Ce is calculated by the recovered magma water contents (based on all cpx with Mg# > 75) and the Ce concentration in the bulk rock. The bulk Ce concentration data are from Zeng *et al.* [2011]. 2 and 3, D<sub>Ce</sub> and D<sub>H2O</sub> are the partition coefficient of Ce and H<sub>2</sub>O between cpx and basaltic melts, which are calculated based on equation (10) in O'Leary *et al.* [2010] and equation (298), (302), (314), and (248) in Bédard [2014]. 4, H<sub>2</sub>O/Ce ratio is calculated by (C<sub>H2O</sub> cpx/D<sub>H2O</sub>)/(C<sub>Ce</sub>/D<sub>Ce</sub>).

[Michael, 1995; Dixon and Clague, 2001; Dixon *et al.*, 2002; Nichols *et al.*, 2002; Simons *et al.*, 2002; Hauri *et al.*, 2006; Workman *et al.*, 2006]. In the following discussion, the H<sub>2</sub>O/Ce ratio will be used to infer the discussion of the mantle source.

On one hand, we calculated H<sub>2</sub>O/Ce ratios based on the estimated magma water content (Table 2) and the Ce content measured for the bulk rock [Zeng *et al.*, 2011]. On the other hand, we calculated the H<sub>2</sub>O/Ce ratio of the melt equilibrium with several specific cpx phenocrysts in the samples FYS10 and FYS07, based on the H<sub>2</sub>O and Ce concentrations in cpx phenocrysts and their partition coefficients (the partition coefficient for Ce is the average value of the results calculated from Equations 298, 302, 314 and 248 in Bédard (2014). The H<sub>2</sub>O partition coefficient is from Equation 10 in O'Leary *et al.* [2010]). We could not apply this calculation for all of the cpx in these two samples because many of them have been destroyed or lost during the separation from thin sections, mounting and polishing processes necessary for SIMS analysis. A comparison of these calculated results is provided in Table 3. Note that the selected cpx in FYS10 have nearly covered the entire range of water contents and Mg# values defined by the cpx in this sample (Table 3 and the Data Set S3). For sample FYS10, the H<sub>2</sub>O/Ce ratio of melt calculated from this approach varies from 333 to 787 (average 546), straddling the H<sub>2</sub>O/Ce calculated by the average meltwater content and the Ce concentration in bulk rock, 696. For FYS7, the H<sub>2</sub>O/Ce ratios of melt calculated by this approach are 105 and 86, with an average of 95, comparable with the ratios calculated by Ce in bulk rock (128). Within the uncertainty of the calculated water content, these two approaches lead to consistent H<sub>2</sub>O/Ce ratio estimations in magma. Thus, we suggest that the estimation of H<sub>2</sub>O/Ce ratios of the "primary" magma based on bulk rock Ce concentration would not lead to larger deviations. In the following discussion, we only use H<sub>2</sub>O/Ce ratios based on the Ce concentration of bulk rock.

Although the residual eclogite model by Zeng *et al.* [2011] could explain the decoupling of εHf and εNd and relatively high <sup>87</sup>Sr/<sup>86</sup>Sr, it cannot explain the observed high H<sub>2</sub>O/Ce ratios. For comparison, the possible H<sub>2</sub>O/Ce ratio of the residual eclogite was calculated. We assume that the eclogite had a water content as high as 3070 ppm prior to the first melting stage [Katayama *et al.*, 2006], which is the highest water content observed in eclogites in continental subduction zones and contains water as structural water in both nominally anhydrous minerals (omphacite, garnet, and rutile) and hydrous minerals, and a Ce concentration of 46 ppm [Qiu *et al.*, 2006; Wang *et al.*, 2009]. This represents the average value of low-εNd eclogites in the Sulu orogeny in Zeng's model. Note that we did not use the published water data obtained using the TC-EA technique [Chen *et al.*, 2007a, 2007b], which may lead to large biases when garnet and omphacite contain retrograded minerals and fluid inclusions. Furthermore, we assume that the water partition coefficient between the eclogite and melt is 0.033 (calculated from D<sup>cpx/melt</sup> and D<sup>grt/melt</sup> of 0.04 and 0.00857, respectively [Hauri *et al.*, 2006] and the modal abundance of 0.75 (cpx) and 0.25 (grt), respectively). After 55% to 60% melting

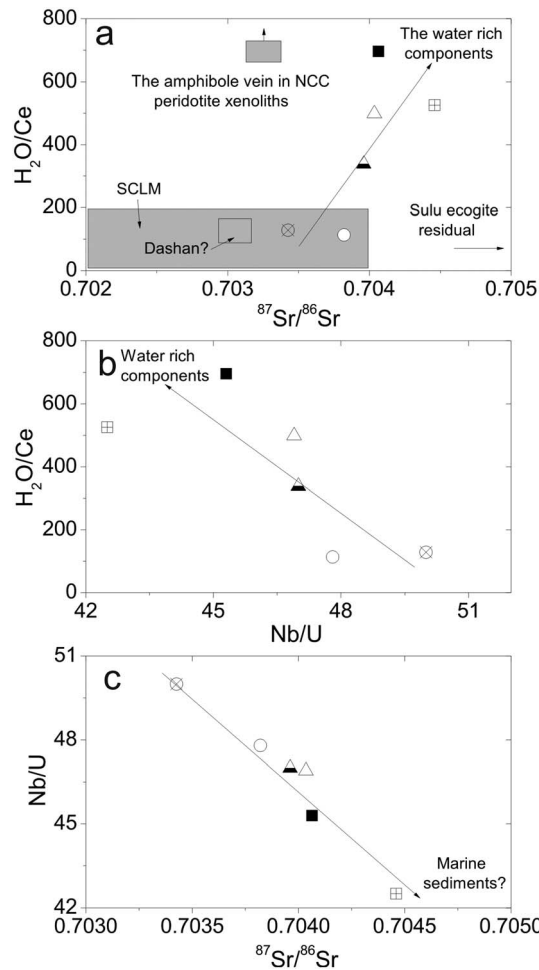


**Figure 13.** (a and b) Comparison of  $H_2O/Ce$  with  $^{87}Sr/^{86}Sr$  and  $Nb/U$  of the bulk rock.  $H_2O/Ce$  of the residual Sulu eclogites is 67, calculated using a water content of 3070 ppm [Katayama et al., 2006] and  $Ce$  of 46 ppm [averaged value of the low- $\epsilon$ Nd eclogites in the Sulu orogen; data from Qiu et al., 2006; Wang et al., 2009].  $H_2O/Ce$  of the Dashan end-member is assumed to be the same as that of FYS07. The  $^{87}Sr/^{86}Sr$  ranges of amphibole in the lithospheric mantle are from Xu and Bodinier [2004] and Xiao et al. [2010]. "SCLM" is the subcontinental lithospheric mantle in eastern NCC, and its  $H_2O/Ce$  ratios were calculated from the published water content data [Xia et al., 2010, 2012; Hao et al., 2012; Li et al., 2014] and the unpublished trace element data of our group. The initial  $^{87}Sr/^{86}Sr$  (at 220 Ma) of eclogite is from 0.706 to 0.710, which is represented by the eclogites in the Sulu-Dabie orogeny [Jahn, 1998; G. C. Zhao et al., 2005; Z. F. Zhao et al., 2005]. Note that the  $^{87}Sr/^{86}Sr$  values were not calculated to the time of the eruption of the Shandong basalts, which would not change any conclusions in this study.

2010; Yang et al., 2008]. Some of the mantle-derived xenoliths contain hydrous minerals, such as mica and amphibole, and their  $^{87}Sr/^{86}Sr$  ratios range from 0.702613 to 0.703284. In addition, the trace element patterns are HFSE depleted [Xu and Bodinier, 2004; Xiao et al., 2010], which is contrary to the observed positive trend between  $H_2O/Ce$  and  $^{87}Sr/^{86}Sr$  in our samples (Figure 13a).

The mantle transition zone beneath Northeast China was believed to be hydrated [Karato, 2011]. Zhao et al. [2009] and Richard and Iwamori [2010] found a prominent low-velocity anomaly from the upper mantle down to approximately 410 km beneath the Changbai volcano. They explained this anomaly as a hot, wet mantle

(with batch melting, which reduces the water content more slowly than other methods, such as fractional melting), the residual eclogites contained water contents of 0.0183 to 0.0168 wt.%; at 20 Ma, melting of these residual eclogites could produce melts with water contents only up to 0.37 wt.%, and the  $H_2O/Ce$  ratio would be similar to its original value (when  $D_{Ce}$  varies from 0.04 to 0.16, the  $H_2O/Ce$  ratio varies from ~67 to ~134). Although the  $H_2O/Ce$  of the Dashan end-member could not be directly constrained here, due to lacking a sample from Dashan, it would exhibit the  $H_2O/Ce$  ratio of sample FYS7, given that (1) the FYS7 was the product of ~10% partial melting of a mantle source similar to the Dashan end-member [Zeng et al., 2011] (Figure 12), and (2) the  $H_2O/Ce$  ratio would not change during partial melting [Michael, 1995; Dixon and Clague, 2001]. As shown in Figure 13a, the trend between  $H_2O/Ce$  and  $^{87}Sr/^{86}Sr$  indicates that mixing of melts derived from mantle sources, such as Dashan and residual Sulu eclogite, could not lead to such water-rich magmas.

**5.3.2.2. The Source of Water: Hydrous Fluids From the Mantle Transition Zone?**

Because shallow crustal processes and the Sulu eclogite have only slight effects on the water content of magmas (see the discussion above), the water-rich component may likely be linked to a hydrous mineral vein in the lithospheric mantle or hydrous melts derived from the mantle transition zone (MTZ), which were triggered by the subducted Pacific slab.

The lithospheric mantle is likely not responsible for the high magma water. Although, in the early Cretaceous, the water content of the lithospheric mantle in the east NCC was estimated to be higher than 1000 ppm [Xia et al., 2013], in the late Cretaceous it has been reduced to 21–231 ppm, and in the Cenozoic the water contents was mainly lower than 50 ppm [Li et al., 2015; Xia et al.,

upwelling arising from an extensive hydrated MTZ. Based on the spatial correlation between basalt geochemistry (such as Ba/Th and Pb/U ratios) and the distribution of the low-velocity zone, *Kuritani et al.* [2011] suggested a direct linkage between the hydrous MTZ and the volcanism at the surface. The authors attributed the high Ba/Th and  $^{207}\text{Pb}/^{206}\text{Pb}$  of these basalts to the breakdown of ancient sediments, which were stagnant in the MTZ and introduced by an ancient subduction event. This event was triggered by the fluid/hydrous melt released by the stagnant subducted Pacific slab. It further explained the hydrous nature of the MTZ beneath east China as the result of these two hydration events. Recently, the basalt lavas at the Wudalianchi in NE China and the Chugaryeong volcano in Korea were also suggested to derive from the mantle source that has been metasomatized by the similar hydrous fluxing from the MTZ [*Kuritani et al.*, 2013; *Sakuyama et al.*, 2014]. Using the same method as this study, *Chen et al.* [2015] investigated the water content of the Shuangliao basalts (51–41 Ma) in Northeast China (near to the Changbai volcano), whose mantle source was suggested to contain components from the stagnant Pacific slab stagnating in the MTZ [*Y. G. Xu et al.*, 2012]. The estimated water contents ranged from 0.9 to 3.09 wt.%, clearly higher than those of MORBs and OIBs [0.1–0.3 wt.% and 0.3–1.0 wt.%, respectively. *Asimow et al.*, 2004; *Michael*, 1988, 1995; *Dixon and Clague*, 2001; *Simons et al.*, 2002; *Wallace*, 1998]. In addition, they found that the  $\text{H}_2\text{O}/\text{Ce}$  ratio of bulk rock was positively correlated with the Ba/Th ratio, but negatively correlated with the Ce/Pb ratio, which confirms that those MTZ components are hydrous and sediment related.

There are several geochemical characteristics of the FYS basalts indicating that their high water contents were derived from the hydrous MTZ with subducted ancient sediments. First, the  $\text{H}_2\text{O}/\text{Ce}$  ratios positively correlate with  $^{87}\text{Sr}/^{86}\text{Sr}$  and negatively with Nb/U (Figures 13a and 13b) in the FYS basalts, suggesting that the water-rich signature comes from a component with a high  $^{87}\text{Sr}/^{86}\text{Sr}$  and low Nb/U, which is consistent with the characteristics of the sediment. The sediment involvement is also indicated by the perfect negative correlation between  $^{87}\text{Sr}/^{86}\text{Sr}$  and Nb/U (Figure 13c). In the contrast, the low  $\text{H}_2\text{O}/\text{Ce}$  components and  $^{87}\text{Sr}/^{86}\text{Sr}$ , coupled with a higher Nb/U ratio, are likely from the subducted oceanic igneous crust, which experienced extensive dehydration during subduction. Although the recycled pyroxenitic cumulates in the mantle can also explain the low  $\text{H}_2\text{O}/\text{Ce}$  ratios [*Bizimis and Pessler*, 2015], the oxygen isotope anomaly of cpx phenocrysts in our sample point to the role of components from the recycled oceanic crust (see the discussion of  $\delta^{18}\text{O}$  in section 5.3.1). Second, the positive Ba and Sr spikes in the primitive mantle normalized pattern of our samples are consistent with those of their counterparts in NE China and Korea [*Kuritani et al.*, 2011, 2013; *Sakuyama et al.*, 2014]. Third, the decoupling of  $\epsilon\text{Hf}$  and  $\epsilon\text{Nd}$  may be a clue that links the samples to ancient marine sediments [*Chauvel et al.*, 2008], although *Zeng et al.* [2011] attributed this isotopic decoupling to the involvement of the Sulu eclogite in the mantle source. In the following section, we present the details of our modeling calculations to suggest that ancient marine sediment could be responsible for these results.

### 5.3.2.3. An Alternative Explanation for $\epsilon\text{Hf}$ - $\epsilon\text{Nd}$ Decoupling: The Role of Marine Sediments

Marine sediments, which have relatively high  $^{176}\text{Hf}/^{177}\text{Hf}$  ratios for a given  $^{143}\text{Nd}/^{144}\text{Nd}$  compared to mantle arrays defined by global OIB and MORB [*Chauvel et al.*, 2008], could cause  $\epsilon\text{Hf}$  and  $\epsilon\text{Nd}$  decoupling in the Shandong basalts (Figure 2b) if they were incorporated into their mantle sources. Here we test the validity of the ancient marine sediments to explain the Hf-Nd isotope decoupling found in the FYS basalts.

To test this possibility, we created a forward modeling calculation of the Sr-Nd-Hf isotopes and trace element patterns (Figure 14) using the Excel spreadsheets from *Stracke et al.* [2003]. The details of the calculation and relevant parameters are shown in Text S2 in the supporting information. We assumed that the Shandong basalts were formed by the mixing of two end-member magmas. One is the Dashan nephelinite, which exhibits an  $^{87}\text{Sr}/^{86}\text{Sr}$  ratio of  $\sim 0.7033$ ,  $\epsilon\text{Nd}$  of 5.8,  $\epsilon\text{Hf}$  of 8.3 and a typical OIB-like trace element pattern (Figure 14b). This end-member lava was generally thought to genetically associate with the mixing of DMM and recycled Pacific oceanic igneous crust [*Z. Xu et al.*, 2012; *Sakuyama et al.*, 2013; *Z. Xu et al.*, 2014]. This is consistent with the cpx  $\delta^{18}\text{O}$  anomaly in sample FYS07 (as low as 3.5‰), which exhibits the same Sr-Nd-Hf isotopes as the Dashan nephelinite (Figures 2a and 2b). The other is the partial melt from a mantle source composed of a solid mixing between the DM mantle and the subducted oceanic sediments (we call this source “DMMsed”). As shown in Figures 14a and 14c, the spread of Nd-Hf and Sr-Nd isotopes in the Shandong basalts can be simulated using the mixing of Dashan nephelinite and the partial melts from the “DMMsed” source, when the oceanic sediment was assumed to be Mariana oceanic sediments at the 800 site [*Plank and Langmuir*, 1998]. In addition, as shown in Figure 14b, for the sample with lowest  $\epsilon\text{Nd}$  (–1.4) in the

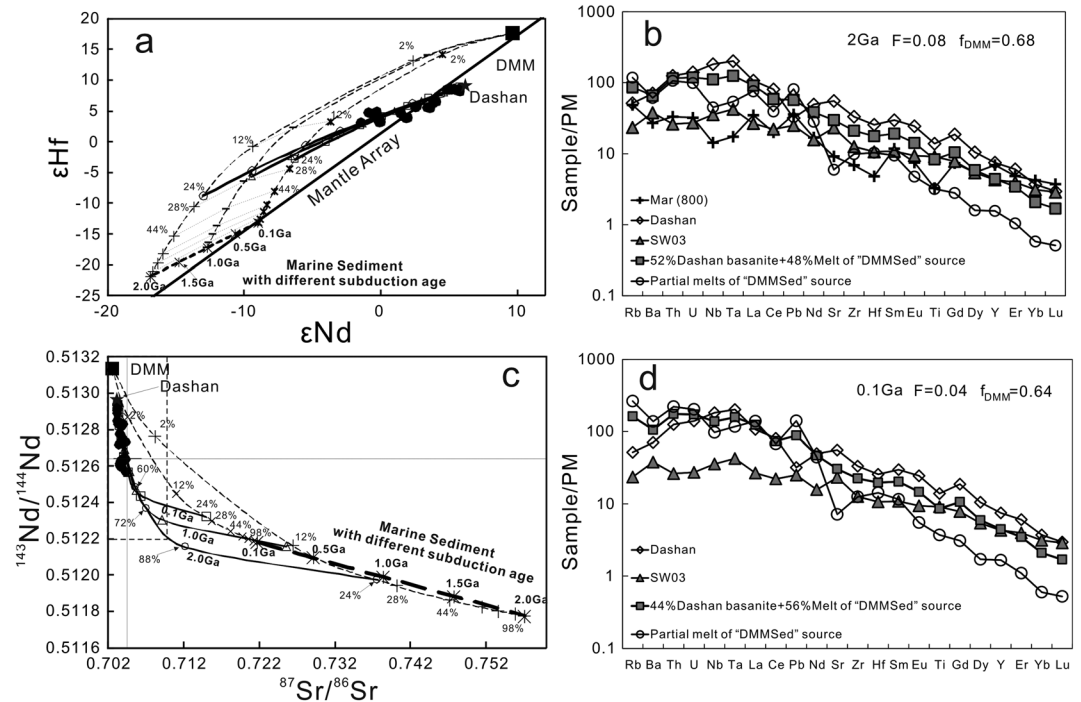


**Figure 14.** Modeling of the Sr-Nd-Hf isotopes and trace element patterns of the Shandong basalts. The isotopic compositions of Shandong basalts are plotted as real black circles. The Sr-Nd-Hf isotopic compositions of DMM and Dashan nephelinite are from *Workman and Hart* [2005] and *Luo et al.* [2009], respectively, and are plotted as real black square and star. The trace element concentration of oceanic sediment is represented by the present-day ODP 800 Site sediments [*Plank and Langmuir*, 1998], and that of Dashan nephelinite is from *Luo et al.* [2009]. In Figures 14a and 14c, the thin dashed lines are the mixing trajectories between the ambient DMM and those ancient sediments, and the thin real dark lines are the mixing trajectories between the Dashan nephelinite and the partial melts of the “DMMSed” source; the numbers show the weight percent of sediments in the mixing. In Figures 14b and 14d, 2 Ga and 0.1 Ga show the time of subduction of the marine sediments (at ODP 800). *F* is the degree of partial melting of the “DMMSed” source, and  $f_{DMM}$  is the proportion of the DM mantle in the solid mixing to form “DMMSed” source. The detailed model calculation and parameters used are presented in Text S2 and Table S2 in the supporting information.

sample group by *Zeng et al.* [2011], SW03, the modeled trace element pattern of the mixed magma, is relatively consistent with its measured bulk rock data.

In summary, although choosing the Mariana oceanic sediments at ODP site 800 seems arbitrary, our modeling produces a scenario where the marine sediment could be responsible for the decoupling of Hf-Nd isotopes in FYS basalts, which is in contrast to the previous suggestion of *Zeng et al.* [2011].

#### 5.4. Comparison With Global OIB H<sub>2</sub>O/Ce Systematics

The H<sub>2</sub>O/Ce of global OIB and plume-influenced MORB vary over a wide range. Specifically, the EM-I type hotspot lavas of the Pitcairn and Koolau end-members in Hawaii exhibit H<sub>2</sub>O/Ce values of ~80 and ~111, respectively [*Kendrick et al.*, 2014; *Dixon and Clague*, 2001], while the EM-II type lavas of Samoa and Society exhibit H<sub>2</sub>O/Ce values of ~50–80 [*Workman et al.*, 2006; *Kendrick et al.*, 2014, 2015]. In contrast, the HIMU type lavas have a higher H<sub>2</sub>O/Ce of ~200, and FOZO type components in the Atlantic and Pacific plume-influenced MORB have H<sub>2</sub>O/Ce values of >250 and ~210, respectively [*Dixon et al.*, 2002; *Métrich et al.*, 2014; *Cabral et al.*, 2014]. Thus, it is clear that the EM-type lavas have the lowest H<sub>2</sub>O/Ce ratios.

Although the trace element patterns and radiogenic isotopes of the FYS are similar to the enriched type OIBs, their H<sub>2</sub>O/Ce ratios (113 to 696, see Table 3) are considerably higher. Similarly, the H<sub>2</sub>O/Ce ratios of Shuangliao basalts (in Northeast China), which exhibit HIMU-like trace element patterns but not very radiogenic Pb isotopes [*Z. Xu et al.*, 2012], range from 133 to 700, significantly higher than the H<sub>2</sub>O/Ce of typical HIMU lavas (~200). The low H<sub>2</sub>O/Ce of EM and HIMU type OIB is typically explained by that the recycled components in their mantle source have experienced efficient dehydration during subduction and water loss

through diffusion during the subsequent mantle storage [Dixon *et al.*, 2002; Workman *et al.*, 2006; Kendrick *et al.*, 2014]. The high H<sub>2</sub>O/Ce ratios for the basalts in East China indicate that their mantle sources are obviously “wetter” than those of typical EM and HIMU-type OIBs. This contrast may be explained by the following: (1) the upper mantle in East Asian has been extensively hydrated by multiple subduction events (ancient and recent) (see the discussion in section 5.3.2), (2) the dehydration of the west Pacific slab during the subduction was less efficient, and/or (3) the water loss through diffusion during the mantle storage period was less significant because the subducted Pacific slab (~170 Ma) [Maruyama, 1997] is rather younger than the recycled components responsible for the EM and HIMU OIBs (>1 Ga) [Weaver, 1991]. Overall, the H<sub>2</sub>O/Ce ratios of basalts derived from “enriched” mantle sources are not necessarily low and are correlated with the dehydration history (subduction and subsequent residence in the mantle) of the recycled components in their mantle sources.

## 6. Concluding Remarks

The water contents in the basaltic magmas in Shandong, eastern China, were estimated by averaging the water contents in melt equilibrated with cpx phenocrysts. The estimated magma water contents range from 0.58 wt. % to 3.89 wt.%, and the highest value exceeds that of normal MORB and OIB. In addition, the H<sub>2</sub>O/Ce ratio for bulk rock can reach 696. The high water content and high H<sub>2</sub>O/Ce in the mantle source indicate that a water-rich component was involved in the source for the Shandong basalts. Such a high water content and H<sub>2</sub>O/Ce cannot be explained by the extremely dry residual Sulu eclogite or the Cenozoic lithospheric mantle represented by peridotite xenoliths. The in situ oxygen analysis showed that the δ<sup>18</sup>O values of the cpx phenocrysts were heterogeneous (from 3.6‰ to 6.3‰) and that most were lower than those derived from a normal mantle or mantle-derived basalt (5.6 ± 0.2‰). These δ<sup>18</sup>O anomalies were not derived from the assimilation of continental crust or the involvement of low δ<sup>18</sup>O eclogite in the Sulu orogeny, thus reflecting an incorporation of components from a subducted oceanic crust, most likely from the stagnant Pacific slab in the MTZ.

In contrast to Zeng's suggestion that the decoupling of εHf and εNd in the Shandong basalts could be exclusively caused by the involvement of residual Sulu eclogite, our detailed modeling calculation indicates that this decoupling can be explained by the addition of marine sediments, which does not cause a substantially high Sr isotopic composition or HFSE depletion. Combined with the similar trace element patterns from the Cenozoic lavas in Northeast China and Korea, the Hf-Nd isotope decoupling and high water content values indicate that the component of the ancient subducted sediments triggered by the stagnant Pacific slab in the mantle source would be present in the mantle source of FYS basalts. The H<sub>2</sub>O/Ce ratios in these OIB-like basalts are much higher than those of typical EM and HIMU type OIBs, which may indicate the net dehydration efficiency of recycled west Pacific slab is low. In addition, it underlines the importance of understanding specific recycling histories (subduction and subsequent residence in the mantle) and their impact on the “wetness” of OIB sources.

## Acknowledgments

The data supporting this paper are available as supporting information. We thank Chen L.H. for providing the Shandong basalts. Jannick Ingrin and István Kovács improved the early manuscript. We thank Y.L. Niu for the helpful comments. The comments from Editor Michael Walter, Takeshi Kuritani, and an anonymous reviewer also contribute much to the improvement of the paper. This work was funded by the NSFC grants 41225005 and 91014007, and the CAS Special Grant for Postgraduate Research, Innovation and Practice.

## References

- Armstrong, J. T. (1989), *CITZAF: Combined ZAF and Pihro (Z) Electron Beam Correction Programs*, Calif. Inst. Tech., Pasadena, Calif.
- Asimow, P. D., J. E. Dixon, and C. H. Langmuir (2004), A hydrous melting and fractionation model for mid-ocean ridge basalts: Application to the Mid-Atlantic Ridge near the Azores, *Geochem. Geophys. Geosyst.*, 5, Q01E16, doi:10.1029/2003GC000568.
- Bédard, J. H. (2014), Parameterizations of calcic clinopyroxene—Melt trace element partition coefficients, *Geochem. Geophys. Geosyst.*, 15, 303–336, doi:10.1002/2013GC005112.
- Bell, D. R., and G. R. Rossman (1992), Water in Earth's mantle: The role of nominally anhydrous 453 minerals, *Science*, 255, 1391–1397.
- Bell, D. R., P. D. Ihinger, and G. R. Rossman (1995), Quantitative analysis of trace OH in garnet and pyroxenes, *Am. Mineral.*, 80, 465–474.
- Bizimis, M., and A. H. Peslier (2015), Water in Hawaiian garnet pyroxenites: Implications for water heterogeneity in the mantle, *Chem. Geol.*, 397, 61–75.
- Cabral, R. A., M. G. Jackson, K. T. Koga, E. F. Rose-Koga, E. H. Hauri, M. J. Whitehouse, and K. A. Kelley (2014), Volatile cycling of H<sub>2</sub>O, CO<sub>2</sub>, F, and Cl in the HIMU mantle: A new window provided by melt inclusions from oceanic hot spot lavas at Mangaia, Cook Islands, *Geochem. Geophys. Geosyst.*, 15, 4445–4467, doi:10.1002/2014GC005473.
- Chauvel, C., F. Lewin, M. Carpentier, N. T. Arndt, and J. C. Marini (2008), Role of recycled oceanic basalt and sediment in generating the Hf-Nd mantle array, *Nat. Geosci.*, 1, 64–67.
- Chen, H., Q. K. Xia, J. Ingrin, Z. B. Jia, and M. Feng (2015), Changing recycled oceanic components in the mantle source of the Shuangliao Cenozoic basalts, NE China: New constraints from water content, *Tectonophysics*, 650, 113–123, doi:10.1016/j.tecto.2014.07.022.
- Chen, L. H., G. Zeng, S. Y. Jiang, A. W. Hofmann, X. S. Xu, and M. B. Pan (2009), Sources of Anfengshan basalts: Subducted lower crust in the Sulu UHP belt, China, *Earth Planet. Sci. Lett.*, 286, 426–435.
- Chen, R. X., Y. F. Zheng, B. Gong, Z. F. Zhao, T. S. Gao, B. Chen, and Y. B. Wu (2007a), Origin of retrograde fluid in ultrahigh-pressure metamorphic rocks: Constraints from mineral hydrogen isotope and water content changes in eclogite–gneiss transitions in the Sulu orogen, *Geochim. Cosmochim. Acta*, 71, 2299–2325.

- Chen, R. X., Y. F. Zheng, B. Gong, Z. F. Zhao, T. S. Gao, B. Chen, and Y. B. Wu (2007b), Oxygen isotope geochemistry of ultrahigh-pressure metamorphic rocks from 200–4000 m core samples of the Chinese Continental Scientific Drilling, *Chem. Geol.*, *242*, 51–75.
- Chen, Y., A. Provost, P. Schiano, and N. Cluzel (2011), The rate of water loss from olivine-hosted melt inclusions, *Contrib. Mineral. Petrol.*, *162*(3), 625–636.
- Chiba, H., T. Chacko, R. N. Clayton, and J. R. Goldsmith (1989), Oxygen isotope fractionations involving diopside, forsterite, magnetite, and calcite: Application to geothermometry, *Geochim. Cosmochim. Acta*, *53*, 2985–2995.
- Choi, S. H., S. T. Kwon, S. B. Mukasa, and H. Sagong (2005), Sr–Nd–Pb isotope and trace element systematics of mantle xenoliths from Late Cenozoic alkaline lavas, South Korea, *Chem. Geol.*, *221*, 40–64.
- Chu, Z. Y., F. Y. Wu, R. J. Walker, R. L. Rudnick, L. Pitcher, I. S. Puchtel, and S. A. Wilde (2009), Temporal evolution of the lithospheric mantle beneath the eastern North China Craton, *J. Petrol.*, *50*, 1857–1898.
- Dixon, J. E., and D. A. Clague (2001), Volatiles in Basaltic glasses from Loihi Seamount, Hawaii: Evidence for a relatively dry plume component, *J. Petrol.*, *42*, 627–654.
- Dixon, J. E., L. Leist, C. Langmuir, and J. G. Schilling (2002), Recycled dehydrated lithosphere observed in plume-influenced mid-ocean-ridge basalt, *Nature*, *420*, 385–389.
- Dixon, J. E., T. H. Dixon, D. R. Bell, and R. Malservisi (2004), Lateral variation in upper mantle viscosity: Role of water, *Earth Planet. Sci. Lett.*, *222*, 451–467.
- Doucet, L. S., A. H. Peslier, D. A. Ionov, A. D. Brandon, A. V. Golovin, A. G. Goncharov, and I. V. Ashchepkov (2014), High water contents in the Siberian cratonic mantle linked to metasomatism: An FTIR study of Udachnaya peridotite xenoliths, *Geochim. Cosmochim. Acta*, *137*, 159–187.
- Eiler, J. M. (2001), Oxygen isotope variations of basaltic lavas and upper mantle rocks, *Rev. Mineral. Geochem.*, *43*, 319–364.
- Eiler, J. M., K. A. Farley, J. W. Valley, E. Hauri, H. Graig, S. R. Hart, and M. Stolper (1997), Oxygen isotope variations in ocean island basalt phenocrysts, *Geochim. Cosmochim. Acta*, *61*, 2281–2293.
- Eiler, J. M., P. Schiano, N. Kitchen, and E. M. Stolper (2000), Oxygen-isotope evidence for recycled crust in the sources of mid-ocean-ridge basalts, *Nature*, *403*, 530–534.
- Fan, Q. C., and P. R. Hooper (1991), The Cenozoic basaltic rocks of eastern China: Petrology and chemical composition, *J. Petrol.*, *32*, 765–810.
- Férot, A., and N. Bolfan-Casanova (2012), Water storage capacity in olivine and pyroxene to 14 GPa: Implications for the water content of the Earth's upper mantle and nature of seismic discontinuities, *Earth Planet. Sci. Lett.*, *349*, 218–230.
- Fukao, Y., M. Obayashi, H. Inoue, and M. Nishii (1992), Subducting slabs stagnant in the mantle transition zone, *J. Geophys. Res.*, *97*(B4), 4809–4822, doi:10.1029/91JB02749.
- Gaetani, G. A., J. A. O'Leary, N. Shimizu, C. E. Bucholz, and M. Newville (2012), Rapid reequilibration of H<sub>2</sub>O and oxygen fugacity in olivine-hosted melt inclusions, *Geology*, *40*(10), 915–918.
- Garth, T., and A. Rietbrock (2014), Order of magnitude increase in subducted H<sub>2</sub>O due to hydrated normal faults within the Wadati-Benioff zone, *Geology*, *42*, 207–210.
- Grant, K., J. Ingrin, J. P. Lorand, and P. Dumas (2007), Water partitioning between mantle minerals from peridotite xenoliths, *Contrib. Mineral. Petrol.*, *154*, 15–34.
- Griffin, W. L., Z. Andi, S. Y. O'Reilly, and C. G. Ryan (1998), Phanerozoic evolution of the lithosphere beneath the Sino-Korean Craton, in *Mantle Dynamics and Plate Interactions in East Asia*, vol. 27, edited by M. F. J. Flower et al., pp. 107–126, AGU, Washington, D. C.
- Guo, P. Y., et al. (2014), Lithosphere thinning beneath west North China Craton: Evidence from geochemical and Sr–Nd–Hf isotope compositions of Jining basalts, *Lithos*, *202–203*, 37–54.
- Gurenko, A. A., I. N. Bindeman, and M. Chaussidon (2011), Oxygen isotope heterogeneity of the mantle beneath the Canary Island: Insights from olivine phenocrysts, *Contrib. Mineral. Petrol.*, *162*, 349–363.
- Hao, Y. T., Q. K. Xia, S. C. Liu, M. Feng, and Y. P. Zhang (2012), Recognizing juvenile and relict 486 lithospheric mantle beneath the North China Craton: Combined analysis of H<sub>2</sub>O, major and trace elements and Sr–Nd isotope compositions of clinopyroxenes, *Lithos*, *149*, 136–145.
- Hauri, E. H., G. A. Gaetani, and T. H. Green (2006), Partitioning of water during melting of the Earth's upper mantle at H<sub>2</sub>O-undersaturated conditions, *Earth Planet. Sci. Lett.*, *248*, 715–734.
- Hong, L. B., Y. H. Zhang, S. P. Qian, J. Q. Liu, Z. Y. Ren, and Y. G. Xu (2013), Constraints from melt inclusions and their host olivines on the petrogenesis of Oligocene–Early Miocene Xindian basalts, Chifeng area, North China Craton, *Contrib. Mineral. Petrol.*, *165*, 305–326.
- Huang, J. L., and D. P. Zhao (2006), High-resolution mantle tomography of China and surrounding regions, *J. Geophys. Res.*, *111*, B09305, doi:10.1029/2005JB004066.
- Huang, J., Y. F. Zheng, Z. F. Zhao, Y. B. Wu, J. B. Zhou, and X. M. Liu (2006), Melting of subducted continent: Element and isotopic evidence for a genetic relationship between Neoproterozoic and Mesozoic granitoids in the Sulu orogen, *Chem. Geol.*, *229*, 227–256.
- Huang, X. L., Y. L. Niu, Y. G. Xu, J. L. Ma, H. N. Qiu, and J. W. Zhong (2013), Geochronology and geochemistry of Cenozoic basalts for eastern Guangdong, SE China: Constraints on the lithosphere evolution beneath the northern margin of the South China Sea, *Contrib. Mineral. Petrol.*, *165*, 437–455.
- Ingrin, J., and H. Skogby (2000), Hydrogen in nominally anhydrous upper-mantle minerals: 499 concentration levels and implications, *Euro. J. Mineral.*, *12*, 543–570.
- Jahn, B. M. (1998), Geochemical and isotope characteristics of UHP eclogites and ultramafic rocks of the Dabie Orogen: Implications for continental subduction and collisional tectonics, in *When Continents Collide: Geodynamics and Geochemistry of Ultrahigh-Pressure Rocks*, pp. 203–239, Kluwer, Dordrecht, Netherlands.
- Karato, S. I. (2011), Water distribution across the mantle transition zone and its implications for global material circulation, *Earth Planet. Sci. Lett.*, *301*, 413–423.
- Katayama, I., S. Nakashima, and H. Yurimoto (2006), Water content in natural eclogite and implication for water transport into the deep upper mantle, *Lithos*, *86*, 245–259.
- Kendrick, M. A., M. G. Jackson, A. J. Kent, E. H. Hauri, P. J. Wallace, and J. Woodhead (2014), Contrasting behaviours of CO<sub>2</sub>, S, H<sub>2</sub>O and halogens (F, Cl, Br, and I) in enriched-mantle melts from Pitcairn and Society seamounts, *Chem. Geol.*, *370*, 69–81.
- Kendrick, M. A., M. G. Jackson, E. H. Hauri, and D. Phillips (2015), The halogen (F, Cl, Br, I) and H<sub>2</sub>O systematics of Samoan lavas: Assimilated-seawater, EM2 and high-<sup>3</sup>He/<sup>4</sup>He components, *Earth Planet. Sci. Lett.*, *410*, 197–209.
- Kovács, I., J. Hermann, H. S. C. O'Neill, J. F. Gerald, M. Sambridge, and G. Horvath (2008), Quantitative absorbance spectroscopy with unpolarized light: Part II. Experimental evaluation and development of a protocol for quantitative analysis of mineral IR spectra, *Am. Mineral.*, *93*, 765–778.
- Kuritani, T., E. Ohtani, and J. I. Kimura (2011), Intensive hydration of the mantle transition zone beneath China caused by ancient slab stagnation, *Nat. Geosci.*, *4*(10), 713–716.

- Kuritani, T., J. I. Kimura, E. Ohtani, H. Miyamoto, and K. Furuyama (2013), Transition zone origin of potassic basalts from Wudalianchi volcano, northeast China, *Lithos*, *156*, 1–12.
- Li, H. Y., X. L. Huang, and H. Guo (2014), Geochemistry of Cenozoic basalts from the Bohai Bay Basin: Implications for a heterogeneous mantle source and lithospheric evolution beneath the eastern North China, *Lithos*, *196–197*, 54–66.
- Li, P., Q. K. Xia, E. Deloule, H. Chen, X. Y. Gu, and M. Feng (2015), Temporal variation of H<sub>2</sub>O content in the lithospheric mantle beneath the eastern North China Craton: Implications for the destruction of cratons, *Gondwana Res.*, *28*, 276–287.
- Libowitzky, E., and G. R. Rossman (1996), Principles of quantitative absorbance measurements in anisotropic crystals, *Phys. Chem. Mineral.*, *23*, 319–327.
- Liu, C. Q., A. Masuda, and G. H. Xie (1994), Major- and trace-element compositions of Cenozoic basalts in eastern China: Petrogenesis and mantle source, *Chem. Geol.*, *114*, 19–42.
- Liu, J., Q. K. Xia, E. Deloule, J. Ingrin, H. Chen, and M. Feng (2015), Water content and oxygen isotopic composition of alkali basalts from the Taihang Mountains, China: Recycled oceanic components in the mantle source, *J. Petrol.*, *56*, 681–702.
- Liu, Y. S., S. Gao, P. Kelemen, and W. L. Xu (2008), Recycled crust controls contrasting source compositions of Mesozoic and Cenozoic basalts in the North China Craton, *Geochim. Cosmochim. Acta*, *72*, 2349–2376.
- Luo, D., L. H. Chen, and G. Zeng (2009), Genesis of intra-continental strongly alkaline volcanic rocks: A case study of Dashan nephelinites in Wudi, Shandong Province, N. China [in Chinese], *Acta Petrol. Sin.*, *25*, 311–319.
- Maruyama, S. (1997), Pacific-type orogeny revisited: Miyashiro-type orogeny proposed, *Island Arc*, *6*, 91–120.
- Mattey, D., D. Lowry, and C. Macpherson (1994), Oxygen isotope composition of mantle peridotite, *Earth Planet. Sci. Lett.*, *128*, 231–241.
- McDonough, W. F., and S. S. Sun (1995), Composition of the Earth, *Chem. Geol.*, *120*, 223–253.
- Meng, F., S. Gao, Y. Niu, Y. Liu, and X. Wang (2014), Mesozoic–Cenozoic mantle evolution beneath the North China Craton: A new perspective from Hf–Nd isotopes of basalts, *Gondwana Res.*, doi:10.1016/j.gr.2014.01.014.
- Menzies, M. A., W. M. Fan, and M. Zhang (1993), Paleozoic and Cenozoic lithoprobes and the loss of >120 km of Archean lithosphere, Sino-Korean craton, China, in *Magmatic Processes and Plate Tectonics*, edited by H. M. Prichard, pp. 71–81, Geol. Soc., London.
- Menzies, M. A., Y. G. Xu, H. F. Zhang, and W. M. Fan (2007), Integration of geology, geophysics and geochemistry: A key to understanding the North China Craton, *Lithos*, *96*, 1–21.
- Métrich, N., V. Zanon, L. Créon, A. Hildenbrand, M. Moreira, and F. O. Marques (2014), Is the 'Azores hotspot' a wetspot? Insights from the geochemistry of fluid and melt inclusions in olivine of Pico basalts, *J. Petrol.*, *55*(2), 377–393.
- Michael, P. J. (1988), The concentration, behavior and storage of H<sub>2</sub>O in the suboceanic upper mantle: Implications for mantle metasomatism, *Geochim. Cosmochim. Acta*, *52*, 555–566.
- Michael, P. J. (1995), Regionally distinctive sources of depleted MORB: Evidence from trace elements and H<sub>2</sub>O, *Earth Planet. Sci. Lett.*, *131*, 301–320.
- Mosenfelder, J. L., and G. R. Rossman (2013), Analysis of hydrogen and fluorine in pyroxenes: II. Clinopyroxene, *Am. Mineral.*, *98*, 1042–1054.
- Nazzareni, S., H. Skogby, and P. F. Zanaz (2011), Hydrogen content in clinopyroxene phenocrysts from Salina mafic lavas (Aeolian arc, Italy), *Contrib. Mineral. Petrol.*, *162*, 275–288.
- Nelson, D. R., A. R. Chivas, B. W. Chappell, and M. T. McCulloch (1988), Geochemical and isotopic systematics in carbonatites and implications for the evolution of ocean-island sources, *Geochim. Cosmochim. Acta*, *52*, 1–17.
- Nichols, A. R. L., M. R. Carroll, and A. Hoskuldsson (2002), Is the Iceland hot spot also wet? Evidence from the water contents of undegassed submarine and subglacial pillow basalts, *Earth Planet. Sci. Lett.*, *202*, 77–87, doi:10.1016/S0012-821X(02)00758-6.
- Niu, Y. L. (2005), Generation and evolution of basaltic magmas: Some basic concepts and a new view on the origin of Mesozoic-Cenozoic basaltic volcanism in eastern China, *Geol. J. China Univ.*, *11*, 9–46.
- O'Leary, J. A., G. A. Gaetani, and E. H. Hauri (2010), The effect of tetrahedral Al<sup>3+</sup> on the partitioning of water between clinopyroxene and silicate melt, *Earth Planet. Sci. Lett.*, *297*, 111–120.
- Peng, Z. C., R. E. Zartman, K. Futa, and D. G. Chen (1986), Pb-, Sr- and Nd-isotopic systematics and chemical characteristics of Cenozoic basalts, eastern China, *Chem. Geol.*, *59*, 3–33.
- Peslier, A. H., J. F. Luhr, and J. Post (2002), Low water contents in pyroxenes from spinel-peridotites of the oxidized, sub-arc mantle wedge, *Earth Planet. Sci. Lett.*, *201*, 69–86.
- Pilet, S., M. B. Baker, and E. M. Stolper (2008), Metasomatized lithosphere and the origin of alkaline lavas, *Science*, *320*, 916–919.
- Plank, T., and C. H. Langmuir (1998), The chemical composition of subducting sediment and its consequences for the crust and mantle, *Chem. Geol.*, *145*(3), 325–394.
- Plank, T., K. A. Kelley, M. M. Zimmer, E. H. Hauri, and P. J. Wallace (2013), Why do mafic arc magmas contain ~4 wt% water on average?, *Earth Planet. Sci. Lett.*, *364*, 168–179.
- Qiu, J. S., R. C. Wang, S. Y. Jiang, J. Hu, X. L. Zhang, and P. Ni (2006), Geochemical comparison between high-Ti and low-Ti eclogites from the main hole of the Chinese Continental Scientific Drilling Project and its implications for rutile mineralization, *Acta Petrol. Sin.*, *22*, 1875–1882.
- Richard, G. C., and H. Iwamori (2010), Stagnant slab, wet plumes and Cenozoic volcanism in East Asia, *Phys. Earth. Plane. Int.*, *183*, 280–287.
- Roeder, P., and R. F. Emslie (1970), Olivine-liquid equilibrium, *Contrib. Mineral. Petrol.*, *29*, 275–289.
- Sakuyama, T., et al. (2013), Recycling and melting of dehydrated oceanic crust from the stagnant slab and contribution from the hydrated mantle transition zone in off-arc mantle: Constraints from Cenozoic alkaline basalts in eastern China, *Chem. Geol.*, *356*, 32–48.
- Sakuyama, T., S. Nagaoka, T. Miyazaki, Q. Chang, T. Takahashi, Y. Hirahara, and K. Ozawa (2014), Melting of the uppermost metasomatized asthenosphere triggered by fluid fluxing from ancient subducted sediment: Constraints from the quaternary basalt lavas at Chugaryeong Volcano, Korea, *J. Petrol.*, *55*(3), 499–528.
- Sambridge, M., J. F. Gerald, I. Kovács, H. S. C. O'Neill, and J. Hermann (2008), Quantitative absorbance spectroscopy with unpolarized light: Part I. Physical and mathematical development, *Am. Mineral.*, *93*(5–6), 751–764.
- Savage, B. (2012), Seismic constraints on the water flux delivered to the deep Earth by subduction, *Geology*, *40*, 235–238.
- Shaw, A. M., E. H. Hauri, M. D. Behn, D. R. Hilton, C. G. Macpherson, and J. M. Sinton (2012), Long-term preservation of slab signatures in the mantle inferred from hydrogen isotopes, *Nat. Geosci.*, *5*, 224–228.
- Simons, K., Dixon, J., Schilling, J. G., Kingsley, R., and Poreda, R. (2002), Volatiles in basaltic glasses from the Easter-Salas y Gomez Seamount Chain and Easter Microplate: Implications for geochemical cycling of volatile elements, *Geochem. Geophys. Geosyst.*, *3*(7), 1020, doi:10.1029/2001GC000173.
- Skogby, H., and G. R. Rossman (1989), OH in pyroxene: An experimental study of incorporation mechanisms and stability, *Am. Mineral.*, *74*, 1059–1069.
- Skogby, H., D. R. Bell, and G. R. Rossman (1990), Hydroxide in pyroxene: Variations in the natural-environment, *Am. Mineral.*, *75*, 764–774.
- Stracke, A., M. Bizimis, and V. J. Salters (2003), Recycling oceanic crust: Quantitative constraints, *Geochem. Geophys. Geosyst.*, *4*(3), 8003, doi:10.1029/2001GC000223.

- Sundvall, R., and R. Stalder (2011), Water in upper mantle pyroxene megacrysts and xenocrysts: A 598 survey study, *Am. Mineral.*, *96*, 1215–1227.
- Tang, J., Y. F. Zheng, Y. B. Wu, B. Gong, X. Zha, and X. Liu (2008), Zircon U–Pb age and geochemical constraints on the tectonic affinity of the Jiaodong terrane in the Sulu orogen, China, *Precambrian Res.*, *161*, 389–418.
- Tang, Y. J., H. F. Zhang, and J. F. Ying (2006), Asthenosphere–lithospheric mantle interaction in an 605 extensional regime: Implication from the geochemistry of Cenozoic basalts from Taihang Mountains, North China Craton, *Chem. Geol.*, *233*, 309–327.
- Taylor, H. P. (1974), The application of oxygen and hydrogen isotope studies to problems of hydrothermal alteration and ore deposition, *Econ. Geol.*, *69*, 843–883.
- Wade, J. A., T. Plank, E. H. Hauri, K. A. Kelly, K. Roggensack, and M. Zimmer (2008), Prediction of magmatic water contents via measurement of H<sub>2</sub>O in clinopyroxene phenocrysts, *Geology*, *36*, 799–802.
- Wallace, P. J. (1998), Water and partial melting in mantle plumes: Inferences from the dissolved H<sub>2</sub>O concentrations of Hawaiian basaltic magmas, *Geophys. Res. Lett.*, *25*, 3639–3642, doi:10.1029/98GL02805.
- Wang, Q., L. Burlini, D. Mainprice, and Z.-Q. Xu (2009), Geochemistry, petrofabrics and seismic properties of eclogites from the Chinese Continental Scientific Drilling boreholes in the Sulu UHP terrane, eastern China, *Tectonophysics*, *475*, 251–266.
- Wang, X. C., S. A. Wilde, Q. L. Li, and Y. N. Yang (2015), Continental flood basalts derived from the hydrous mantle transition zone, *Nat. Commun.*, *6*, 7700, doi:10.1038/ncomms8700.
- Wang, Y., Z.-F. Zhao, Y.-F. Zheng, and J.-J. Zhang (2011), Geochemical constraints on the nature of mantle source for Cenozoic continental basalts in east-central China, *Lithos*, *125*, 940–955.
- Weaver, B. L. (1991), The origin of ocean island basalt end-member compositions: Trace element and isotopic constraints, *Earth Planet. Sci. Lett.*, *104*(2), 381–397.
- Widom, E., and J. Farquhar (2003), Oxygen isotope signatures in olivines from São Miguel (Azores) basalts: Implications for crustal and mantle processes, *Chem. Geol.*, *193*, 237–255.
- Winpenny, B., and J. MacLennan (2014), Short length scale oxygen isotope heterogeneity in the Icelandic mantle: Evidence from plagioclase compositional zones, *J. Petrol.*, *55*, 2537–2566.
- Withers, A. C. (2013), On the use of unpolarized infrared spectroscopy for quantitative analysis of absorbing species in birefringent crystals, *Am. Mineral.*, *98*, 689–697.
- Workman, R. K., and S. R. Hart (2005), Major and trace element composition of the depleted MORB mantle (DMM), *Earth Planet. Sci. Lett.*, *231*, 53–72.
- Workman, R. K., E. H. Hauri, S. R. Hart, J. H. Wang, and J. Blusztajn (2006), Water and trace element in basaltic glasses from Samoa: Implications for water distribution in the mantle, *Earth Planet. Sci. Lett.*, *241*, 932–951, doi:10.1016/j.epsl.2005.10.028.
- Wu, C. Z., I. M. Samson, Z. Y. Chen, L. H. Chen, L. X. Gu, G. G. Gai, J. Li, and G. D. Yang (2014), Ar–Ar dating and Sr–Nd–Pb isotopic character of Paleogene basalts from the Xialiaohu Depression, northern Bohai Bay Basin: Implications for transformation of the subcontinental lithospheric mantle under the eastern North China Craton, *Can. J. Earth Sci.*, *51*, 166–179.
- Xia, Q. K., L. Dallai, and E. Delouie (2004), Oxygen and hydrogen isotope heterogeneity of clinopyroxene megacrysts from Nushan Volcano, SE China, *Chem. Geol.*, *209*, 137–151.
- Xia, Q. K., Y. T. Hao, P. Li, E. Delouie, M. Coltorti, L. Dallai, X. Z. Yang, and M. Feng (2010), Low water content of the Cenozoic lithospheric mantle beneath the eastern part of the North China Craton, *J. Geophys. Res.*, *115*, B07207, doi:10.1029/2009JB006694.
- Xia, Q. K., J. Liu, S. C. Liu, I. Kovács, M. Feng, and L. Dang (2013), High water content in Mesozoic primitive basalts of the North China Craton and implications on the destruction of cratonic mantle lithosphere, *Earth Planet. Sci. Lett.*, *361*, 85–97.
- Xiao, Y., H. F. Zhang, W. M. Fan, J. F. Ying, J. Zhang, X. M. Zhao, and B. X. Su (2010), Evolution of lithospheric mantle beneath the Tan-Lu fault zone, eastern North China Craton: Evidence from petrology and geochemistry of peridotite xenoliths, *Lithos*, *117*, 229–246.
- Xu, Y. G., and J. L. Bodinier (2004), Contrasting enrichments in high- and low-temperature mantle xenoliths from Nushan, Eastern China: Results of a single metasomatic event during lithospheric accretion?, *J. Petrol.*, *45*, 321–341.
- Xu, Y. G., J. L. Ma, F. A. Frey, M. D. Feigenson, and J. F. Liu (2005), Role of lithosphere–asthenosphere interaction in the genesis of Quaternary alkalic and tholeiitic basalts from Datong, western North China Craton, *Chem. Geol.*, *224*, 247–271.
- Xu, Y. G., H. H. Zhang, H. N. Qiu, W. C. Ge, and F. Y. Wu (2012), Oceanic crust components in continental basalts from Shuangliao, Northeast China: Derived from the mantle transition zone?, *Chem. Geol.*, *328*, 168–184.
- Xu, Z., Z. F. Zhao, and Y. F. Zheng (2012), Slab–mantle interaction for thinning of cratonic lithospheric mantle in North China: Geochemical evidence from Cenozoic continental basalts in central Shandong, *Lithos*, *146*, 202–217.
- Xu, Z., Y. F. Zheng, Z. F. Zhao, and B. Gong (2014), The hydrous properties of subcontinental lithospheric mantle: Constraints from water content and hydrogen isotope composition of phenocrysts from Cenozoic continental basalts in North China, *Geochim. Cosmochim. Acta*, *143*, 285–302, doi:10.1016/j.gca.2013.12.025.
- Yang, X. Z., Q. K. Xia, E. Delouie, L. Dallai, Q. C. Fan, and M. Feng (2008), Water in minerals of the continental lithospheric mantle and overlying lower crust: A comparative study of peridotite and granulite xenoliths from the North China Craton, *Chem. Geol.*, *256*, 33–45.
- Yu, S. Y., Y. G. Xu, J. L. Ma, Y. F. Zheng, Y. S. Kuang, L. B. Hong, and L. X. Tong (2010), Remnants of oceanic lower crust in the subcontinental lithospheric mantle: Trace element and Sr–Nd–O isotope evidence from aluminous garnet pyroxenite xenoliths from Jiaohe, Northeast China, *Earth Planet. Sci. Lett.*, *297*, 413–422.
- Zeng, G., L. H. Chen, X. S. Xu, S. Y. Jiang, and A. W. Hofmann (2010), Carbonated mantle sources for Cenozoic intra-plate alkaline basalts in Shandong, North China, *Chem. Geol.*, *273*, 35–45.
- Zeng, G., L. H. Chen, A. W. Hofmann, and X. S. Xu (2011), Crust recycling in the sources of two parallel volcanic chains in Shandong, North China, *Earth Planet. Sci. Lett.*, *302*, 359–368.
- Zhang, J. J., Y. F. Zheng, and Z. F. Zhao (2009), Geochemical evidence for interaction between oceanic crust and lithospheric mantle in the origin of Cenozoic continental basalts in east-central China, *Lithos*, *110*, 305–326.
- Zhang, W. H., H. F. Zhang, W. M. Fan, B. F. Han, and M. F. Zhou (2012), The genesis of Cenozoic basalts from the Jining area, northern China: Sr–Nd–Pb–Hf isotope evidence, *J. Asian Earth Sci.*, *61*, 128–142.
- Zhang, Z. M., K. Shen, J. L. Wang, and H. L. Dong (2009), Petrological and geochronological constraints on the formation, subduction and exhumation of the continental crust in the southern Sulu orogen, eastern-central China, *Tectonophysics*, *475*, 291–307.
- Zhao, D. P., Y. Tian, J. S. Lei, L. Liua, and S. H. Zheng (2009), Seismic image and origin of the Changbai intraplate volcano in East Asia: Role of big mantle wedge above the stagnant Pacific slab, *Phys. Earth Planet. Inter.*, *173*, 197–206.
- Zhao, G. C., M. Sun, S. A. Wilde, and S. Z. Li (2005), Late Archean to Paleoproterozoic evolution of the North China Craton: Key issues revisited, *Precambrian Res.*, *136*, 177–202.
- Zhao, Y. W., Q. C. Fan, H. B. Zou, and N. Li (2014), Geochemistry of Quaternary basaltic lavas from the Nuomin volcanic field, Inner Mongolia: Implications for the origin of potassic volcanic rocks in Northeastern China, *Lithos*, *196–197*, 169–180.
- Zhao, Z. F., and Y. F. Zheng (2003), Calculation of oxygen isotope fractionation in magmatic rocks, *Chem. Geol.*, *193*, 59–80.

- Zhao, Z. F., Y. F. Zheng, B. Chen, and Y. B. Wu (2005), A geochemical study of element and Sr-Nd isotopes for eclogite and gneiss from CCSD core 734 to 933m, *Acta. Petrol. Sin.*, *21*, 325–338.
- Zheng, Y. F. (1991), Calculation of oxygen isotope fractionation in metal oxides, *Geochim. Cosmochim. Acta*, *55*, 2299–2307.
- Zheng, Y. F., B. Fu, B. Gong, and L. Li (2003), Stable isotope geochemistry of ultrahigh pressure metamorphic rocks from the Dabie–Sulu orogen in China: Implications for geodynamics and fluid regime, *Earth Sci. Rev.*, *62*, 105–161.
- Zhi, X. C., Y. Song, F. A. Frey, J. L. Feng, and M. Z. Zhai (1990), Geochemistry of Hannuoba basalts, eastern China: Constraints on the origin of continental alkali and tholeiitic basalt, *Chem. Geol.*, *66*(88), 1–33.
- Zhou, X., and R. L. Armstrong (1982), Cenozoic volcanic rocks of eastern China: Secular and geographic trends in chemistry and strontium isotopic composition, *Earth Planet. Sci. Lett.*, *58*, 301–329.
- Zou, H. B., A. Zindler, X. S. Xu, and Q. Qi (2000), Major, trace element, and Nd, Sr and Pb isotope studies of Cenozoic basalts in SE China: Mantle sources, regional variations, and tectonic significance, *Chem. Geol.*, *171*, 33–34.
- Zou, H. B., C. C. Shen, and Q. C. Fan (2014), U-series disequilibrium in young Tengchong volcanics: Recycling of mature clay sediments or mudstones into the SE Tibetan mantle, *Lithos*, *192*, 132–141.